Post-Print

Unexpected collision detection, estimation and reaction for a free-flying orbital robot

Francesco Cavenago * and Mauro Massari †
Polytechnic University of Milan, Milan, 20156, Italy

Alessandro M. Giordano ‡ and Gianluca Garofalo §
German Aerospace Center, Oberpfaffenhofen-Weßling, Starnberg, 82234, Germany

This paper addresses the unexpected contact handling problem for a free-flying orbital robot. A nonlinear observer is developed to detect, isolate and estimate a collision. Then, a reaction control strategy is proposed, which aims at avoiding the build-up of the contact force and possible instabilities. It is proved that the controlled system is input-to-state stable. The performance of the observer and the controller is assessed through a numerical example featuring a 7 degrees-of-freedom arm mounted on a spacecraft and a realistic measurement model. The spacecraft is equipped with thrusters and variable speed control moment gyros.

I. Introduction

On-orbit servicing missions have been a long-term goal since their first conceptual designs in the early 1980s, with the ARAMIS project[1]. However, after almost 40 years, the use of orbital robots is still very limited. The major experiences are the ones related to the space shuttle and the International Space Station (ISS)[2–5]. The first OOS demonstration mission can be dated 1997: the Experimental Test Satellite VII (ETS-VII)[6] of the JAXA. A 6-degrees-of-freedom (DoF) manipulator was mounted on an unmanned vehicle and autonomous rendezvous and docking, teleoperation and servicing tasks were verified. Another demonstration mission was the Orbital Express[7] in 2007 by the Defense Advanced Research Project Agency (DARPA), in which different technologies for autonomous servicing, such as docking, refueling, and ORU replacement were tested. Despite the potential of robotic technologies for OOS missions, after this latter experience, no other space robotic arms for servicing have been launched. The reason lies in the high complexity involved in this kind of missions, especially if the system is required to be autonomous. Several technological challenges have to be faced and overcome. Among them, one of the most critical is to deal with physical contacts between the free-flying orbital robot and a possible target object, which could be unknown and uncooperative.

The dynamics of the contact phase has been extensively studied, considering in particular free-floating robots[8–11].

---
*Postdoctoral Researcher, Department of Aerospace Science and Technology, francesco.cavenago@polimi.it .
†Associate professor, Department of Aerospace Science and Technology, mauro.massari@polimi.it.
‡Associate Researcher, Institute of Robotics and Mechatronics, alessandro.giordano@dlr.de.
§Associate Researcher, Institute of Robotics and Mechatronics, gianluca.garofalo@dlr.de.

Moreover, many authors have addressed the problem of guaranteeing a safe interaction when the robot's end-effector comes into contact with the target[12–15]. In these works, a nominal capture operation is considered, in which the robot has to perform planned grasping tasks and the goal of the controller is to keep a stable contact in order to enable the correct capture of the target. Conversely, this paper focuses on unexpected collisions that may occur during the on-orbit proximity operations as well. Imagine a mission involving an unknown and uncooperative target. The algorithm responsible for the shape reconstruction may fail in identifying some appendages, which can collide with the manipulator moving nearby. Another example is given by a scenario in which the robot could move close to several objects, and a wrong estimation of the relative distances could lead to an unplanned collision. These are only a couple of examples of off-nominal situations that can happen, but many others can be visualized. Therefore, the space robot should be endowed with algorithms to handle contacts, which can occur unexpectedly along its entire structure.

Collision handling has been extensively studied for several years within the robotics community, especially for fixed-base manipulators[16, 17], humanoids[18, 19] and flying robots[20, 21]. On the other hand, to the best of the authors' knowledge, this problem for free-flying orbital robots has not been addressed so far. Along the same line of [16], contact handling can be divided into different phases:

- **Contact detection**: the goal of this phase is to detect whether a contact occurred or not. A signal, whose modulus is expected to lie below a certain threshold, is monitored and, whenever an unexpected change happens, an alarm is risen.

- **Contact isolation**: this phase aims at locating the exact point of the contact along the robot, or at least the part involved.

- **Contact identification**: in this phase the contact force is estimated, which is a valuable information that may be exploited in the implementation of control strategies to guarantee a safe physical interaction.

- **Contact reaction**: in this last phase the robot is controlled to react properly to the external disturbance caused by the contact, avoiding multiple impacts and possible instabilities.

In order to address the first three phases jointly, one could think to use tactile sensors, such as sensitive skins, as proposed for some terrestrial robotic applications [22–24]. However, in a space scenario, it is obviously more practical and convenient to detect, isolate and estimate a collision without using additional and dedicated sensors, which result in a higher cost and power demand. For this reason, in [25], the authors propose a nonlinear observer to estimate an external wrench acting at a generic point along the robot. This scheme is an extension to floating-base robot of the well-known and well-established momentum-based observer initially developed for fixed-base robot[26]. Three residual vectors are defined as the difference between the real and estimated linear, angular and joints momentum, respectively. Under ideal conditions, two residual vectors turn out to be an estimation of the force and moment acting at the center of mass (CoM) of the robot due to the contact. The last one is an estimate of the contact disturbance torques at the joint level. The three residuals can be used to detect and isolate the contact, and, moreover, they can be exploited to

reconstruct the entire contact wrench. However, in [25], the linear momentum residual is shown to be sensitive to noise and uncertainties in the measurements, with consequent deterioration of the wrench reconstruction performance. This is mainly due to the dependence of this residual on the satellite linear velocity, which is difficult to acquire accurately at high frequency. Therefore, from a practical point of view, it is more convenient to use only the angular and joints momentum residuals for the contact detection, isolation and identification. Indeed, they provide an accurate estimation since their computation relies on sensors featuring relatively high acquisition frequency and low noise, such as encoders, gyroscopes and joint torque sensors. Further details about this observer can be found in [25]. Also other researchers have proposed observer schemes to estimate a contact force for a space robot. For instance, in [27] the disturbance observer is used, while in [28] the force is reconstructed through the target's equations of motion. However, these methods assume that the contact is at the end-effector during a nominal capture operation. Moreover, they require quantities that are not measured directly, such as the joint accelerations and the linear velocity of robot base for the former, and the target accelerations for the latter. These quantities could be obtained through numerical differentiation, but they would introduce nonnegligible noise in the estimation process.

In this paper, the first three phases of the physical contact handling are addressed redesigning the nonlinear observer [25]. In particular, a different formulation of the system dynamics is used, in which the velocity of the CoM of the whole system, the body-frame angular velocity of the spacecraft and the joint velocities are introduced as new generalized velocities. This new version of the observer is more suitable to be integrated with the reaction control strategy proposed in the paper, which is derived from the same dynamics formulation. Indeed, a compliant controller is developed which regulates the motion of the CoM of the whole system, the spacecraft attitude and the joint positions. The controller commands the robot to move away from the hit obstacle, while keeping or moving to a desired attitude. The escaping direction to follow is provided by the nonlinear observer, which is able to estimate the direction and orientation of the disturbance. Thanks to this strategy, multiple impacts and the build-up of the contact force, which can lead to damages and instability, are avoided. The controller is proved to be input-to-state stable, namely the error on the states is bounded during the contact and goes to zero when the contact ends. Finally, the performance of both observer and reaction control is assessed through a numerical simulation considering a 7DoF arm mounted on a spacecraft, a realistic measurement model and assuming the spacecraft equipped with thrusters and variable speed control moment gyros (VSCMG). Moreover, the developed reaction strategy can be integrated with the controllers proposed in [29, 30] by one of the authors, which are coordinated controllers of the base and end-effector for nominal grasping operations without and with reaction wheels, respectively. The controllers [29, 30] can already handle small contacts avoiding the drift of the base for workspace need. In this paper, riskier contact situations are considered and the integration of these controllers with the proposed reaction strategy is suggested. In particular, the controllers [29, 30] can be used until an unexpected collision occurs, then, if the collision does not satisfy safety criteria, the control authority may be switched to the present reaction control for safety. The main difference of the reaction control compared to [29, 30] is that it

3

works in joints space rather than in task space. In this way, singularity issues are avoided during the escape maneuver and maximum safety is ensured during the risky situation.

To summarize, the main contributions of the paper are: 1) the physical contact handling problem on a generic point is addressed for free-flying orbital robots for the first time; 2) a reaction control strategy to unexpected collisions is developed and proved to be input-to-state stable; 3) the observer presented in [25] is further developed and analyzed considering a more realistic actuation system, namely thrusters and VSCMG.

The paper is organized as follows. Section II provides the main notations and the robot's dynamics. In Section III, the dynamics is reformulated introducing the velocity of the CoM of the whole robot as new generalized velocity. In Section IV, a nonlinear observer is developed based on the dynamics reformulation to address the contact detection, isolation and identification. Then, in Section V, the proposed reaction control is derived and the input-to-state stability is proved. In Section VI the performance of both observer and control is assessed through a numerical example. Finally, in Section VII the limitations of the proposed strategy are discussed and in Section VIII the main conclusions are drawn.

II. Preliminaries

A. Problem statement

The free-flying orbital robot is required to perform servicing operations in orbit. In this context, dealing with physical contact can be necessary. The most common situation is the space robot performing manipulation or grasping tasks, in which the end-effector comes into contact with a target object. However, unexpected collisions may occur as well.

In this study, the space robot is modelled as a multibody system made up of $n + 1$ rigid bodies connected by n revolute joints (see Fig. 1). No environmental disturbances are taken into account (e.g., solar pressure, gravity gradient, air drag and magnetic torques), since they are smaller than the contact and actuation forces. A contact on a generic point along the robot is considered.

B. Main notations

Four main reference frames are defined (see Fig. 1). One, denoted by $\mathcal{B}$, is the body frame located on the center-of-mass (CoM) of the spacecraft. The second one, denoted by $\mathcal{C}$, is a non-inertial frame, always parallel to $\mathcal{B}$, placed on the CoM of the space robot. The third one, denoted by $\mathcal{E}$, is a frame located on the end-effector. The last one is the inertial frame, denoted by $\mathcal{T}$.

In order to transform forces and velocities between reference frames, the Adjoint transformation [31] is introduced:
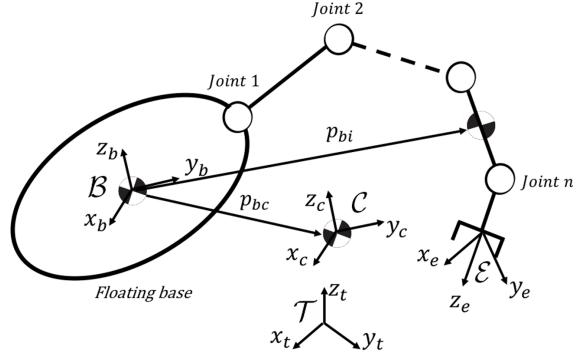
Fig. 1   Floating orbital robot.

$$A_{xy} = \begin{bmatrix} R_{xy} & [p_{xy}]^\wedge R_{xy} \\ 0 & R_{xy} \end{bmatrix} \in \mathbb{R}^{6\times 6}, \tag{1}$$

where $p_{xy} \in \mathbb{R}^3$ and $R_{xy} \in \mathrm{SO}(3)$ indicate the generic position vector, expressed in $\mathcal{X}$, and rotation matrix from frame $\mathcal{X}$ to frame $\mathcal{Y}$, respectively. The operator $[\,\cdot\,]^\wedge$ stands for the skew-symmetric matrix of the argument. Finally, the identity matrix and zero matrix are denoted by E and 0 of suitable dimensions, respectively.

C. Robot dynamics during the contact phase

The dynamics of the free-flying robot during the contact phase can be expressed as follows:

$$\underbrace{\begin{bmatrix} M_t & M_{tr} & M_{tm} \\ M_{tr}^T & M_r & M_{rm} \\ M_{tm}^T & M_{rm}^T & M_m \end{bmatrix}}_{M(q)} \begin{bmatrix} \dot{v}_b \\ \dot{\omega}_b \\ \ddot{q} \end{bmatrix} + \underbrace{\begin{bmatrix} C_t & C_{tr} & C_{tm} \\ C_{rt} & C_r & C_{rm} \\ C_{mt} & C_{mr} & C_m \end{bmatrix}}_{C(q,\dot{q},v_b,\omega_b)} \begin{bmatrix} v_b \\ \omega_b \\ \dot{q} \end{bmatrix} = \begin{bmatrix} f_b \\ m_b \\ \tau \end{bmatrix} + \begin{bmatrix} f_{ext,b} \\ m_{ext,b} \\ \tau_{ext} \end{bmatrix}, \tag{2}$$

where

$$\begin{bmatrix} f_{ext,b} \\ m_{ext,b} \\ \tau_{ext} \end{bmatrix} = \begin{bmatrix} A_{pb}^T \\ J_p^T \end{bmatrix} \mathcal{F}_{ext}, \tag{3}$$

and where

$\mathcal{F}_{ext} = [f_{ext}^T \ m_{ext}^T]^T \in \mathbb{R}^6$ is the contact wrench at a generic point p along the robot,

$J_p \in \mathbb{R}^{6 \times n}$ is the fixed-base robot's Jacobian for the point p,

$v_b, \omega_b \in \mathbb{R}^3$ are the linear and angular velocity of the base expressed in $\mathcal{B}$,

$q, \dot{q} \in \mathbb{R}^n$ are the joint angles and velocities,

$f_b, m_b \in \mathbb{R}^3$ are the commanded base force and torque around $\mathcal{B}$, expressed in $\mathcal{B}$,

$\tau \in \mathbb{R}^n$ are the commanded joint torques,

$M_t, M_{tr}, M_r \in \mathbb{R}^{3 \times 3}$ are submatrices that compose the inertia matrix of the composite rigid body,

$M_{tm}, M_{rm} \in \mathbb{R}^{3 \times n}$ are the coupling inertia matrices,

$M_m \in \mathbb{R}^{n \times n}$ is the inertia matrix of the manipulator,

$C(q, \dot{q}, v_b, \omega_b) \in \mathbb{R}^{(6+n) \times (6+n)}$ is the Coriolis/centrifugal matrix.

The analytical expression of the inertia matrix $M(q)$ can be found in [32].

D. Definitions and theorem for the input-to-state stability

Consider the following generic dynamic system:

$$\dot{x} = f(x, u)$$
$$y = h(x, u)$$

(4)

where $x \in \mathbb{R}^n$, $u \in \mathbb{R}^m$, and $y \in \mathbb{R}^g$ are the state vector, input vector and output vector, respectively.

Definition 1 [33] The system (4) is Input-to-State Stable (ISS) if there exist functions * $\beta \in \mathcal{KL}$ and $\gamma \in \mathcal{K}$ such that

$$|x(t, x_0, u)| \leq \beta(|x_0|, t) + \gamma(\sup(|u|))$$

(5)

for all $t \geq 0$, $x_0 \in \mathbb{R}^n$, and u. An equivalent condition for the ISS [34] is the existence of a differentiable function V: $\mathbb{R}^n \to \mathbb{R}$ such that $\alpha_1(|x|) \leq V(x) \leq \alpha_2(|x|)$ for some $\alpha_1, \alpha_2 \in \mathcal{K}_\infty$, and satisfying for all x, u

$$\dot{V} \leq -\gamma(|x|) + \sigma(|u|)$$

(6)

where $\gamma \in \mathcal{K}_\infty$ and $\sigma \in \mathcal{K}$. The function V is called an ISS-Lyapunov function.

Definition 2 [34] The system (4) admits an Input-Output-to-State-Stable Lyapunov function (IOSS-Lyapunov) if

---

*A scalar continuous function $\alpha(r)$, defined for $r \in [0, a)$, belongs to class $\mathcal{K}$ if it is strictly increasing and $\alpha(0) = 0$; it belongs to class $\mathcal{K}_\infty$ is it is defined for all $r \geq 0$ and $\alpha(r) \to \infty$ as $r \to \infty$. A scalar function $\beta(r, s)$, defined for $r \in [0, a)$ and $s \in [0, \infty)$, belongs to class $\beta \in \mathcal{KL}$ if, for each fixed s, the mapping $\beta(r, s)$ belongs to $\mathcal{K}$ with respect to r and, for each fixed r, the mapping $\beta(r, s)$ is decreasing with respect to s and $\beta(r, s) \to 0$ as $s \to \infty$.

there exist a differentiable V: $\mathbb{R}^n \to \mathbb{R}$ such that $\alpha_1(|\boldsymbol{x}|) \le V(\boldsymbol{x}) \le \alpha_2(|\boldsymbol{x}|)$ for some $\alpha_1, \alpha_2 \in \mathcal{K}_\infty$, and for all $\boldsymbol{x}, \boldsymbol{u}$:

$$\dot{V} \le -\gamma(|\boldsymbol{x}|) + \sigma(|\boldsymbol{u}|) + \lambda(|\boldsymbol{y}|) \tag{7}$$

where $\sigma, \lambda \in \mathcal{K}$ and $\gamma \in \mathcal{K}_\infty$.

Definition 3 [34] The system (4) admits a quasi ISS Lyapunov function (qISS-Lyapunov) if there exist a differentiable V: $\mathbb{R}^n \to \mathbb{R}$ such that $\alpha_1(|\boldsymbol{x}|) \le V(\boldsymbol{x}) \le \alpha_2(|\boldsymbol{x}|)$ for some $\alpha_1, \alpha_2 \in \mathcal{K}_\infty$, and for all $\boldsymbol{x}, \boldsymbol{u}$:

$$\dot{V} \le -\bar{\gamma}(|\boldsymbol{y}|) + \sigma(|\boldsymbol{u}|) \tag{8}$$

where $\sigma, \bar{\gamma} \in \mathcal{K}_\infty$.

Theorem 1 [34] The system (4) is Input-to-State Stable provided that:

- it admits a qISS-Lyapunov function: $\dot{V}_1 \le -\bar{\gamma}(|\boldsymbol{y}|) + \sigma_1(|\boldsymbol{u}|)$

- it admits a IOSS-Lyapunov function: $\dot{V}_2 \le -\gamma(|\boldsymbol{x}|) + \sigma_2(|\boldsymbol{u}|) + \lambda(|\boldsymbol{y}|)$

- $\limsup\limits_{r \to \infty} \lambda(r)/\bar{\gamma}(r) < +\infty$

III. Decoupled translational and rotational dynamics

In this paragraph the dynamics (2) is reformulated substituting the velocity of the base $\boldsymbol{v}_b$ with the velocity of the center of mass of the whole system, expressed in $\mathcal{T}$. In this way, it is possible to obtain a decoupling of the translational dynamics from the rotational dynamics of the base and the joints dynamics. In the following sections, it will be shown that this feature provides some useful advantages in the observer design.

Introducing the velocity of the center of mass of the whole system in the inertial frame, denoted by $\boldsymbol{v}_c \in \mathbb{R}^3$, the following transformation, through the matrix $\boldsymbol{\Gamma} \in \mathbb{R}^{(6+n)\times(6+n)}$, can be defined:

$$\begin{bmatrix} \boldsymbol{v}_c \\ \boldsymbol{\omega}_b \\ \dot{\boldsymbol{q}} \end{bmatrix} = \underbrace{\begin{bmatrix} \boldsymbol{R}_{tb} & -\boldsymbol{R}_{tb}[\boldsymbol{p}_{bc}]^\wedge & \boldsymbol{R}_{tb}\bar{\boldsymbol{J}}_v \\ \boldsymbol{0} & \boldsymbol{E} & \boldsymbol{0} \\ \boldsymbol{0} & \boldsymbol{0} & \boldsymbol{E} \end{bmatrix}}_{\boldsymbol{\Gamma}} \begin{bmatrix} \boldsymbol{v}_b \\ \boldsymbol{\omega}_b \\ \dot{\boldsymbol{q}} \end{bmatrix}, \tag{9}$$

where

$$\bar{\boldsymbol{J}}_v = \frac{1}{m}\boldsymbol{M}_{tm} \in \mathbb{R}^{3\times n}, \tag{10}$$

and where $m \in \mathbb{R}$ is the total mass of the satellite-manipulator ensemble. Consequently, the generalized forces transform as

$$\begin{bmatrix} f_b \\ m_b \\ \tau \end{bmatrix} = \mathbf{\Gamma}^T \begin{bmatrix} f_t \\ m_c \\ \tau^* \end{bmatrix}, \tag{11}$$

$$\begin{bmatrix} f_{ext,b} \\ m_{ext,b} \\ \tau_{ext} \end{bmatrix} = \mathbf{\Gamma}^T \begin{bmatrix} f_{ext,t} \\ m_{ext,c} \\ \tau^*_{ext} \end{bmatrix}, \tag{12}$$

where $f_t \in \mathbb{R}^3$, $m_c \in \mathbb{R}^3$, and $\tau^* \in \mathbb{R}^n$ are new control inputs; $f_{ext,t} \in \mathbb{R}^3$, $m_{ext,c} \in \mathbb{R}^3$, and $\tau^*_{ext} \in \mathbb{R}^n$ are the generalized external forces in the new variables space.

Then, the dynamics in the new generalized velocities is derived pre-multiplying (2) by $\mathbf{\Gamma}^{-T}$ and substituting v_b, ω_b, $\dot{q}$ and their derivatives computed from Eq. (9) in (2). The resulting system is

$$\begin{bmatrix} mE & \mathbf{0} & \mathbf{0} \\ \mathbf{0} & I_c & I_c \bar{J}_\omega \\ \mathbf{0} & \bar{J}_\omega^T I_c^T & \tilde{M}_m \end{bmatrix} \begin{bmatrix} \dot{v}_c \\ \dot{\omega}_b \\ \ddot{q} \end{bmatrix} + \begin{bmatrix} \mathbf{0} & \tilde{C}_{cr} & \tilde{C}_{cm} \\ -\tilde{C}_{cr}^T & \tilde{C}_r & \tilde{C}_{rm} \\ -\tilde{C}_{cm}^T & \tilde{C}_{mr} & \tilde{C}_m \end{bmatrix} \begin{bmatrix} v_c \\ \omega_b \\ \dot{q} \end{bmatrix} = \begin{bmatrix} f_t \\ m_c \\ \tau^* \end{bmatrix} + \begin{bmatrix} f_{ext,t} \\ m_{ext,c} \\ \tau^*_{ext} \end{bmatrix}, \tag{13}$$

where $I_c \in \mathbb{R}^{3\times 3}$ is the rotational inertia around C of the whole body, and where

$$\bar{J}_\omega = \left(M_r - \frac{1}{m} M_{tr}^T M_{tr} \right)^{-1} \left(M_{rm} - \frac{1}{m} M_{tr}^T M_{tm} \right) \in \mathbb{R}^{3\times n}, \tag{14}$$

$$\tilde{M}_m = M_m - \frac{1}{m} M_{tm}^T M_{tm} \in \mathbb{R}^{n\times n}. \tag{15}$$

It can be proven (see Appendix) that $\tilde{C}_{cr}\omega_b + \tilde{C}_{cm}\dot{q} = \mathbf{0}$ and

$$-\tilde{C}_{cr}^T v_c + \tilde{C}_r \omega_b + \tilde{C}_{rm}\dot{q} = (\dot{I}_c + [\omega_b]^\wedge I_c)\omega_b + (\dot{I}_c \bar{J}_\omega + I_c \dot{\bar{J}}_\omega + [\omega_b]^\wedge I_c \bar{J}_\omega)\dot{q}, \tag{16a}$$

$$-\tilde{C}_{cm}^T v_c + \tilde{C}_{mr}^T \omega_b + \tilde{C}_m \dot{q} = (\dot{\tilde{M}}_m - \frac{1}{2}\tilde{M}_{rm/q} - \frac{1}{2}\tilde{M}_{m/q})\dot{q} + (\dot{\bar{J}}_\omega^T I_c^T + \bar{J}_\omega^T \dot{I}_c^T + \frac{1}{2}I_{c/q}^{-T}I_c^T - \frac{1}{2}\bar{J}_{\omega/q}^T I_c^T)\omega_b, \tag{16b}$$

where

$$\tilde{M}_{rm/q} = \begin{bmatrix} \omega_b^T \frac{\partial(I_c \bar{J}_\omega)}{\partial q_1} \\ \vdots \\ \omega_b^T \frac{\partial(I_c \bar{J}_\omega)}{\partial q_n} \end{bmatrix}, \quad \tilde{M}_{m/q} = \begin{bmatrix} \dot{q}^T \frac{\partial \tilde{M}_m}{\partial q_1} \\ \vdots \\ \dot{q}^T \frac{\partial \tilde{M}_m}{\partial q_n} \end{bmatrix} \in \mathbb{R}^{n\times n}. \tag{17}$$

8

$$\boldsymbol{I}_{c/q}^{-T} = \begin{bmatrix} (\boldsymbol{\omega}_b + \bar{\boldsymbol{J}}_\omega \dot{\boldsymbol{q}})^T \boldsymbol{I}_c^T \frac{\partial \boldsymbol{I}_c^{-T}}{\partial q_1} \\ \vdots \\ (\boldsymbol{\omega}_b + \bar{\boldsymbol{J}}_\omega \dot{\boldsymbol{q}})^T \boldsymbol{I}_c^T \frac{\partial \boldsymbol{I}_c^{-T}}{\partial q_n} \end{bmatrix}, \quad \bar{\boldsymbol{J}}_{\omega/q}^T = \begin{bmatrix} \dot{\boldsymbol{q}}^T \frac{\partial \bar{\boldsymbol{J}}_\omega^T}{\partial q_1} \\ \vdots \\ \dot{\boldsymbol{q}}^T \frac{\partial \bar{\boldsymbol{J}}_\omega^T}{\partial q_n} \end{bmatrix} \in \mathbb{R}^{n \times 3}. \tag{18}$$

Note that $\bar{\boldsymbol{J}}_{\omega/q}^T$, $\tilde{\boldsymbol{M}}_{m/q}$, $\dot{\bar{\boldsymbol{J}}}_\omega$ and $\dot{\boldsymbol{I}}_c$ are function of $\boldsymbol{q}$ and $\dot{\boldsymbol{q}}$, $\tilde{\boldsymbol{M}}_{rm/q}$ is function of $\boldsymbol{q}$ and $\boldsymbol{\omega}_b$, and $\boldsymbol{I}_{c/q}^{-T}$ is function of $\boldsymbol{q}$, $\dot{\boldsymbol{q}}$ and $\boldsymbol{\omega}_b$. Therefore, the translational dynamics is completely decoupled from the rotational and joints dynamics:

$$m\dot{\boldsymbol{v}}_c = \boldsymbol{f}_t + \boldsymbol{f}_{ext,t}, \tag{19a}$$

$$\boldsymbol{I}_c \dot{\boldsymbol{\omega}}_b + \boldsymbol{I}_c \bar{\boldsymbol{J}}_\omega \ddot{\boldsymbol{q}} + (\dot{\boldsymbol{I}}_c + [\boldsymbol{\omega}_b]^\wedge \boldsymbol{I}_c)\boldsymbol{\omega}_b + (\dot{\boldsymbol{I}}_c \bar{\boldsymbol{J}}_\omega + \boldsymbol{I}_c \dot{\bar{\boldsymbol{J}}}_\omega + [\boldsymbol{\omega}_b]^\wedge \boldsymbol{I}_c \bar{\boldsymbol{J}}_\omega)\dot{\boldsymbol{q}} = \boldsymbol{m}_c + \boldsymbol{m}_{ext,c}, \tag{19b}$$

$$\tilde{\boldsymbol{M}}_m \ddot{\boldsymbol{q}} + \bar{\boldsymbol{J}}_\omega^T \boldsymbol{I}_c^T \dot{\boldsymbol{\omega}}_b + (\dot{\tilde{\boldsymbol{M}}}_m - \frac{1}{2}\tilde{\boldsymbol{M}}_{rm/q} - \frac{1}{2}\tilde{\boldsymbol{M}}_{m/q})\dot{\boldsymbol{q}} + (\dot{\bar{\boldsymbol{J}}}_\omega^T \boldsymbol{I}_c^T + \bar{\boldsymbol{J}}_\omega^T \dot{\boldsymbol{I}}_c^T + \frac{1}{2}\boldsymbol{I}_{c/q}^{-T} \boldsymbol{I}_c^T - \frac{1}{2}\bar{\boldsymbol{J}}_{\omega/q}^T \boldsymbol{I}_c^T)\boldsymbol{\omega}_b = \boldsymbol{\tau}^* + \boldsymbol{\tau}_{ext}^*. \tag{19c}$$

The decoupling between the translational dynamics and the rotational and joints ones is exploited in the following to develop a nonlinear observer for use in the detection, isolation and estimation phases. Moreover, the proposed reaction strategy is based on this decoupled dynamics as well.

IV. Contact detection, estimation and isolation

In order to address the contact detection, isolation and estimation problems jointly, a momentum-residual-based observer for free-flying orbital robots is developed based on the dynamics (19). The design of this observer follows the same idea of the one presented in [25] by the authors. It is an extension to the floating-base case of the well-known momentum-based observer, proposed in [26] for fixed-base robots, in which a residual vector is defined as the difference between the generalized momentum of the robot and its estimate. Under ideal condition, this residual vector turns out to be a filtered estimation of the external disturbance acting on the joints.

Based on (19), three residual vectors $\hat{\boldsymbol{f}}_{ext,t}$, $\hat{\boldsymbol{m}}_{ext,c}$ and $\hat{\boldsymbol{\tau}}_{ext}^*$ can be defined as the difference between the real

momentum and the estimated one:

$$\hat{f}_{ext,t} = K_f (\underbrace{m v_c}_{h_t^t} - \int_0^t (f_t + \hat{f}_{ext,t}) ds), \tag{20a}$$

$$\hat{m}_{ext,c} = K_m (\underbrace{I_c \omega_b + I_c \bar{J}_\omega \dot{q}}_{h_c^r} - \int_0^t (m_c - [\omega_b]^\wedge (I_c \omega_b + I_c \bar{J}_\omega \dot{q}) + \hat{m}_{ext,c}) ds), \tag{20b}$$

$$\hat{\tau}_{ext}^* = K_\tau (\underbrace{\tilde{M}_m \dot{q} + \bar{J}_\omega^T I_c^T \omega_b}_{h_j} - \int_0^t (\tau^* + \frac{1}{2} (\tilde{M}_{m/q} + \tilde{M}_{rm/q}) \dot{q} + \frac{1}{2} (-I_{c/q}^{-T} I_c^T + \bar{J}_{\omega/q}^T I_c^T) \omega_b + \hat{\tau}_{ext}^*) ds), \tag{20c}$$

where $h_t^t \in \mathbb{R}^3$ is the translational momentum of the whole system expressed in $\mathcal{T}$, $h_c^r \in \mathbb{R}^3$ is the rotational momentum of the whole system around C and expressed in C, and $h_j \in \mathbb{R}^3$ is the generalized joints momentum.

Differentiating Eqs. (20a), (20b), and (20c), and using the dynamics (19), the resulting relations between the estimates and the true quantities are

$$\dot{\hat{f}}_{ext,t} = K_f (f_{ext,t} - \hat{f}_{ext,t}), \tag{21a}$$

$$\dot{\hat{m}}_{ext,c} = K_m (m_{ext,c} - \hat{m}_{ext,c}), \tag{21b}$$

$$\dot{\hat{\tau}}_{ext}^* = K_\tau (\tau_{ext}^* - \hat{\tau}_{ext}^*), \tag{21c}$$

meaning that $\hat{f}_{ext,t}$, $\hat{m}_{ext,c}$, and $\hat{\tau}_{ext}^*$ are first-order-filtered estimations of $f_{ext,t}$, $m_{ext,c}$, and τ_{ext}^*, respectively.

Increasing the observer gains reduces the time constants of the transient response of the estimates, and thus a faster estimation of $f_{ext,t}$, $m_{ext,c}$, and τ_{ext}^*. Ideally, if the observer gains tend to infinity, it would be achieved $\hat{f}_{ext,t} \approx f_{ext,t}$, $\hat{m}_{ext,c} \approx m_{ext,c}$ and $\hat{\tau}_{ext}^* \approx \tau_{ext}^*$, respectively. However, in practice, noise and uncertainties induce an upper bound on the values that the observer gains can take. Then, note that the computation of the residual $\hat{f}_{ext,t}$ requires the knowledge of the linear velocity of the spacecraft, which is difficult to acquire accurately and at high frequency in practice. Indeed, no direct measurements are available, and numerical differentiation or estimation are necessary, introducing non-negligible noise and uncertainties in the estimation process of the force. In [25], it is shown that this noise and uncertainties on v_b highly affect the computation of the translational momentum residual, limiting significantly the value of the gain, and thus the bandwidth. Consequently, fast and relatively soft impacts are hardly detected and identified. On the other hand, thanks to the decoupled structure of the dynamics (19), the residuals $\hat{m}_{ext,c}$ and $\hat{\tau}_{ext}^*$ do not depend on the base velocity and can be computed just relying on sensors featuring high acquisition frequency and relatively low noise, such as encoders, gyroscopes, joint torque sensors. Higher gains can be set leading to larger

bandwidths, which means a faster transient and better estimation of the base torque and joint torques due to the contact.

Another aspect to consider is the quality of the wrench reconstruction. Theoretically, the three residuals can be exploited together to reconstruct the external wrench. However, the authors show in [25] that it is better from a practical point of view to reconstruct the wrench using only angular and joints momentum residuals, namely $\hat{m}_{ext,c}$ and $\hat{\tau}^*_{ext}$, without including the translational momentum residual $\hat{f}_{ext,t}^{\dagger}$. Indeed, the latter one introduces in the wrench reconstruction process the noise and uncertainties of the base linear velocity, deteriorating significantly the performance. Moreover, the limited acquisition frequency prevents a good estimation of fast contact. For these reasons, in the following, only $\hat{m}_{ext,c}$ and $\hat{\tau}^*_{ext}$ are considered for the contact detection, isolation and wrench estimation.

A. Detection

In the detection phase, a significant signal for the problem is monitored. This signal is expected to lie below a certain threshold, and when it is not, an alarm is risen. In this case, the components of $\hat{m}_{ext,c}$ and $\hat{\tau}^*_{ext}$ are perfect monitoring signals for the contact detection. Indeed, theoretically, until a collision occurs, all the components are zero. In practice, as already observed, noise and uncertainties affect these signals, and thus a certain threshold for each components must be set. The problem can be stated as follows:

$$\begin{cases} |r_k| < \epsilon_k \rightarrow \text{no collision} \\ |r_k| \geq \epsilon_k \rightarrow \text{collision} \end{cases} \tag{22}$$

where $r_k \in \mathbb{R}$ is a generic component of the residual vectors $\hat{m}_{ext,c}$ and $\hat{\tau}^*_{ext}$, and $\epsilon_k \in \mathbb{R}$ is the related threshold. The choice of the threshold must be made analyzing the effects of noise and uncertainties on the monitored signals. It is a trade-off between sensitivity, which requires a low threshold, and robustness to false positive, which requires a high threshold.

B. Wrench reconstruction

Assuming knowledge of the contact point, once estimates of $f_{ext,t}$, $m_{ext,c}$, and τ^*_{ext} are available, the external wrench $\mathcal{F}_{ext}$ can be estimated. Indeed, using the relations (3) and (12), it is possible to write

---

†The observer derived in [25] is slightly different from the one proposed in this paper since it exploits a different formulation of the dynamics. In particular, the velocity of the CoM expressed in C, the angular momentum around C and expressed in C, and the joints velocity are used as generalized velocities. However, the two observers are related to each other, and the observations made for the one in [25] are valid also here.

$$
\begin{bmatrix} \hat{f}_{ext,t} \\ \hat{m}_{ext,c} \\ \hat{\tau}_{ext}^* \end{bmatrix} = \Gamma^{-T} \begin{bmatrix} A_{pb}^T \\ J_p^T \end{bmatrix} \hat{\mathcal{F}}_{ext} = \underbrace{\begin{bmatrix} R_{pt}^T & 0 \\ [p_{cp}]^\wedge R_{pb}^T & R_{pb}^T \\ J_{vp}^T - \bar{J}_v^T R_{pb}^T & J_{\omega p}^T \end{bmatrix}}_{J_p^{*T} \in \mathbb{R}^{(n+6) \times 6}} \hat{\mathcal{F}}_{ext}, \tag{23}
$$

where $J_{vp}, J_{\omega p} \in \mathbb{R}^{3 \times n}$ are the sub-blocks of $J_p = \begin{bmatrix} J_{vp} & J_{\omega p} \end{bmatrix}$, i.e., the Jacobians mapping $\dot{q}$ into the linear and angular velocity of a frame attached on the contact point p, respectively.

Since $\hat{f}_{ext,t}$ is expected to be particularly corrupted by noise and uncertainties [25], it is better to remove it from the reconstruction process, reducing the relation (23) to

$$
\begin{bmatrix} \hat{m}_{ext,c} \\ \hat{\tau}_{ext}^* \end{bmatrix} = \underbrace{\begin{bmatrix} [p_{cp}]^\wedge R_{pb}^T & R_{pb}^T \\ J_{vp}^T - \bar{J}_v^T R_{pb}^T & J_{\omega p}^T \end{bmatrix}}_{\tilde{J}_p^{*T} \in \mathbb{R}^{(n+3) \times 6}} \hat{\mathcal{F}}_{ext}. \tag{24}
$$

Assuming that $n > 3$ and $\tilde{J}_p^*$ has maximum rank, an estimate of the external wrench $\mathcal{F}_{ext}$ can be computed using only the residuals $\hat{m}_{ext,c}$, and $\hat{\tau}_{ext}^*$ in the following way

$$
\hat{\mathcal{F}}_{ext} = \left(\tilde{J}_p^{*T} \right)^{\#} \begin{bmatrix} \hat{m}_{ext,c} \\ \hat{\tau}_{ext}^* \end{bmatrix}, \tag{25}
$$

where the operator $(\cdot)^{\#}$ stands for the Moore-Penrose pseudo-inverse. It is worth stressing that the use of only $\hat{m}_{ext,c}$, and $\hat{\tau}_{ext}^*$ in the reconstruction process enables to obtain fast and accurate estimation of the external wrench, since it involves high-frequency and relatively low-noise measurements.

Note that Eq.(25) requires the knowledge of the contact point to compute the Jacobian $\tilde{J}_p^*$. In case of an unexpected collision, assuming this knowledge is unrealistic. Therefore, before performing the reconstruction, it is necessary to locate where the collision occurred. To this aim, in the next section, a strategy involving only the rotational and joints momentum residuals, is proposed.

C. Isolation

In the isolation phase, the objective is to locate where a collision occurred along the space robot. In the development of the proposed strategy, it is assumed that the point of application of the external disturbance does not change during the contact and the wrench consists only in a linear force and no torque, namely $\mathcal{F}_{ext} = [f_{ext}^T \ 0^T]^T$. Note that these are

reasonable assumptions for unexpected collisions.

Assuming that the link i_c on which the contact occurred is known, the external wrench $\mathcal{F}_{ext}$ can be transformed with respect to a frame attached on a known position to link i_c using the Adjoint matrix, as

$$
\mathcal{F}_{i_c} = \begin{bmatrix} f_{i_c} \\ m_{i_c} \end{bmatrix} = A^T_{p i_c} \mathcal{F}_{ext} = \begin{bmatrix} E & 0 \\ [p_{i_c p}]^\wedge & E \end{bmatrix} \begin{bmatrix} f_{ext} \\ 0 \end{bmatrix},
\tag{26}
$$

where $p_{i_c p}$ is constant.

The effect of the contact wrench at frame i_c can be estimated using the reconstruction strategy previously explained as

$$
\hat{\mathcal{F}}_{i_c} = \begin{bmatrix} \hat{f}_{i_c} \\ \hat{m}_{i_c} \end{bmatrix} = \left(\begin{bmatrix} [p_{c i_c}]^\wedge R^T_{i_c b} & R^T_{i_c b} \\ J^T_{v i_c} - \bar{J}^T_v R^T_{i_c b} & J^T_{\omega i_c} \end{bmatrix} \right)^\# \begin{bmatrix} \hat{m}_{ext,c} \\ \hat{\tau}^*_{ext} \end{bmatrix},
\tag{27}
$$

where $J_{v i_c}$, $J_{\omega i_c} \in \mathbb{R}^{3 \times n}$ are the Jacobians mapping $\dot{q}$ into the linear and angular velocity of the frame i_c. At this point, by manipulating Eq. (26) the following relation can be written

$$
\hat{m}_{i_c} = [p_{i_c p}]^\wedge \hat{f}_{i_c},
\tag{28}
$$

from which the line of action of f_{ext} can be computed as

$$
s_{i_c p} = (-[\hat{f}_{i_c}]^\wedge)^\# \hat{m}_{i_c} + d_{i_c} \frac{\hat{f}_{i_c}}{\|\hat{f}_{i_c}\|} \in \mathbb{R}^3.
\tag{29}
$$

with $d_{i_c} \in \mathbb{R}$ being a varying scalar. Assuming the knowledge of the geometry of the link i_c, the contact point can be found as the intersection between the link and the line $s_{i_c p}$.

Unfortunately, the contact link is usually not known in advance. However, it is possible to overcome this issue. Indeed, the scheme just explained can be applied to each link, assuming it is the one in contact. At the end, two possible results can be obtained:

- no intersections are found between the line of action and the link;
- a candidate contact point is found.

Among all the candidate points, the real contact point is the one minimizing

$$
\delta_{ip} = \left| \tilde{J}^{*T}_{p,i} \begin{bmatrix} \hat{f}_{ext} \\ 0 \end{bmatrix} - \begin{bmatrix} \hat{m}_{ext,c} \\ \hat{\tau}^*_{ext} \end{bmatrix} \right|,
\tag{30}
$$

where $\tilde{J}_{p,i}^* \in \mathbb{R}^{6 \times (n+3)}$ is the Jacobian at the candidate point on link i. Fig. 2 reports the isolation method schematically.

To summarize, the residuals $\hat{m}_{ext,c}$ and $\hat{\tau}_{ext}^*$ allow not only to detect and reconstruct a contact force, but also to isolate it.

As last remark, note that the isolation strategy proposed in [16] for fixed-base robots can not be applied using the residual $\hat{\tau}_{ext}^*$. In [16], the contact link i_c is identified as the one associated to the last component different from zero of an estimate of τ_{ext}. This feature is not valid anymore when the estimate $\hat{\tau}_{ext}^*$ is used. Indeed, from (12), the following relation results

$$\tau_{ext}^* = \tau_{ext} - \bar{J}_v^T R_{tb}^T \hat{f}_{ext,t}, \tag{31}$$

where it can be clearly observed that τ_{ext} and τ_{ext}^* are not the same quantity. To stress this fact, consider a contact on the base of the robot. The components of τ_{ext} will be all zero. On the contrary, the components of τ_{ext}^* will not, due to the second term in (31). This is also an advantage in the considered example. Indeed, τ_{ext}^* contains useful information for the detection and reconstruction of the contact on the base.
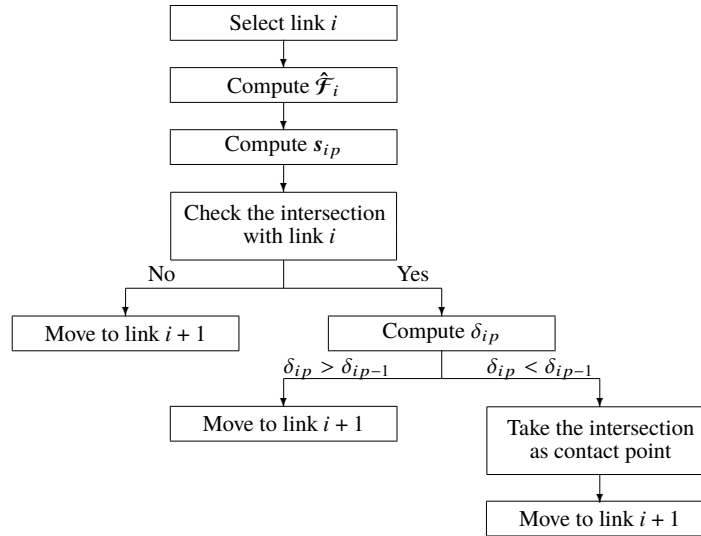
Fig. 2   Scheme of the proposed isolation method.

V. Reaction control strategy

Once the unexpected collision has been detected and identified, the robot should be commanded to react properly in order to avoid other impacts, the build-up of the force and consequently possible instabilities. In the proposed strategy based on the dynamics (19), the CoM of the robot and the manipulator are commanded to move away from the obstacle. Imaging a collision on the robotic arm, the distance between the contact point on the robot and the one on the obstacle

is increased by two actions: a displacement of the entire system and a change of the manipulator configuration. The escape directions to follow can be derived from the force reconstruction and the joint momentum residual, as it will be shown later. On the other hand, the attitude controller is required to keep or to move to a prescribed orientation of the spacecraft. This is motivated by the fact that a desired attitude can be necessary in order to communicate information or to keep a possible target in the field of view of the sensors, e.g. cameras or lidar.

In the following, first, the derivation of the controller is reported and the input-to-state stability of the controlled system during contact is proved. The controller is derived with the assumption that the required state is available. Then, the advantages of the proposed strategy are analyzed. Finally, the introduction of the VSCMG and thrusters as actuators is discussed.

A. Controller derivation

The dynamics (19) can be rewritten in a more compact way as follows:

$$m\dot{v}_c = f_t + f_{ext,t}, \tag{32a}$$

$$M^*\dot{\breve{\omega}} + C^*\breve{\omega} = m^* + m^*_{ext}, \tag{32b}$$

where $\breve{\omega} = [\omega_b^T \ \dot{q}^T]^T \in \mathbb{R}^{3+n}$, $m^* = [m_c^T \ \tau^{*T}]^T \in \mathbb{R}^{3+n}$, $m^*_{ext} = [m_{ext,c}^T \ \tau^{*T}_{ext}]^T \in \mathbb{R}^{3+n}$, and where

$$M^*(q) = \begin{bmatrix} I_c & I_c\bar{J}_\omega \\ \bar{J}_\omega^T I_c^T & \tilde{M}_m \end{bmatrix} \in \mathbb{R}^{(3+n)\times(3+n)}, \tag{33}$$

$$C^*(q,\dot{q},\omega_b) = \begin{bmatrix} \dot{I}_c + [\omega_b]^\wedge I_c & \dot{I}_c\bar{J}_\omega + I_c\dot{\bar{J}}_\omega + [\omega_b]^\wedge I_c\bar{J}_\omega \\ \dot{\bar{J}}_\omega^T I_c^T + \bar{J}_\omega^T \dot{I}_c^T + \frac{1}{2}I_{c/q}^{-T}I_c^T - \frac{1}{2}\bar{J}_{\omega/q}^T I_c^T & \dot{\tilde{M}}_m - \frac{1}{2}\tilde{M}_{rm/q} - \frac{1}{2}\tilde{M}_{m/q} \end{bmatrix} \in \mathbb{R}^{(3+n)\times(3+n)}. \tag{34}$$

Note that, for the dynamics (32b), the property $\breve{\omega}^T(\dot{M}^* - 2C^*)\breve{\omega} = 0$ is valid (see the Appendix for the proof).

A compliant controller for the reaction can be implemented exploiting the new control inputs as follows

$$f_t = -K_c\tilde{x}_c - D_c v_c, \tag{35a}$$

$$m^* = -J_{\tilde{\phi}}^T K^*\tilde{\phi} - D^*\breve{\omega} \tag{35b}$$

where $\tilde{x}_c \in \mathbb{R}^3$ is the error on the position of the CoM of the whole system, $\tilde{\phi}^T = [2\tilde{\epsilon}^T \ \tilde{q}^T]^T \in \mathbb{R}^{3+n}$, with $\tilde{\epsilon} \in \mathbb{R}^3$ being the vector part of the quaternion error extracted from $R_{b_d b} = R_{tb_d}^T R_{tb}$, and $\tilde{q} \in \mathbb{R}^n$ being the joint angles error.

The rotation matrix $\boldsymbol{R}_{tb_d}$ is the desired one. The matrices $\boldsymbol{K}_c, \boldsymbol{D}_c, \boldsymbol{K}^*, \boldsymbol{D}^*$ are positive definite matrices of appropriate dimensions. In addition, $\boldsymbol{K}^*$ is block diagonal, i.e., $\boldsymbol{K}^* = \text{blockdiag}\{\boldsymbol{K}^*_{\tilde{\epsilon}}, \boldsymbol{K}^*_{\tilde{q}}\}$, with $\boldsymbol{K}^*_{\tilde{\epsilon}}, \boldsymbol{K}^*_{\tilde{q}}$ being the attitude stiffness and the joint stiffness, respectively. Finally, $\boldsymbol{J}_{\tilde{\phi}}$ is defined as follows:

$$\dot{\tilde{\boldsymbol{\phi}}} = \boldsymbol{J}_{\tilde{\phi}} \breve{\omega} \tag{36}$$

where

$$\boldsymbol{J}_{\tilde{\phi}} = \begin{bmatrix} (\tilde{\eta}\boldsymbol{E} + [\tilde{\boldsymbol{\epsilon}}]^\wedge) & \boldsymbol{0} \\ \\ \boldsymbol{0} & \boldsymbol{E} \end{bmatrix} \in \mathbb{R}^{(3+n)\times(3+n)}, \tag{37}$$

and where $\tilde{\eta} \in \mathbb{R}$ is the scalar part of the quaternion error.

B. Input-to-state stability of the controlled system

In this section, it is shown the input-to-state stability (ISS) of the controlled orbital robot. Consider the dynamics (32) and the control actions (35), the closed-loop dynamics is

$$m\dot{\boldsymbol{v}}_c + \boldsymbol{D}_c\boldsymbol{v}_c + \boldsymbol{K}_c\tilde{\boldsymbol{x}}_c = \boldsymbol{f}_{ext,t}, \tag{38a}$$

$$\boldsymbol{M}^*\dot{\breve{\omega}} + (\boldsymbol{C}^* + \boldsymbol{D}^*)\breve{\omega} + \boldsymbol{J}^T_{\tilde{\phi}}\boldsymbol{K}^*\tilde{\boldsymbol{\phi}} = \boldsymbol{m}^*_{ext}. \tag{38b}$$

Since the dynamics (38a) and (38b) are decoupled, the stability analysis is carried out separately, one subsystem at time. In both cases, only the regulation problem is considered and it is assumed that the external disturbance due to the contact is bounded. The definitions and the theorem used in the ISS stability proof are reported in Sect. II.D.

Proposition 1: The generalized rotational controlled dynamics of the free-flying orbital robot (38b) is input-to-state stable w.r.t. the input $\boldsymbol{m}^*_{ext}$.

Proof. Consider the following candidate Lyapunov function:

$$V_{r1} = \frac{1}{2}\breve{\omega}^T\boldsymbol{M}^*\breve{\omega} + \frac{1}{2}\tilde{\boldsymbol{\phi}}^T\boldsymbol{K}^*\tilde{\boldsymbol{\phi}}, \tag{39}$$

$$\frac{1}{2}\lambda^*_{min}(\boldsymbol{M}^*, \boldsymbol{K}^*)(|\breve{\omega}|^2 + |\tilde{\boldsymbol{\phi}}|^2) \le V_{r1} \le \frac{1}{2}\lambda^*_{max}(\boldsymbol{M}^*, \boldsymbol{K}^*)(|\breve{\omega}|^2 + |\tilde{\boldsymbol{\phi}}|^2), \tag{40}$$

where $\lambda^*_{min}(\cdot, \circ) = \min(\lambda_{min}(\cdot), \lambda_{min}(\circ))$ and $\lambda^*_{max}(\cdot, \circ) = \max(\lambda_{max}(\cdot), \lambda_{max}(\circ))$, with $\lambda_{min}(\cdot), \lambda_{max}(\cdot)$ being the minimum and maximum eigenvalue of the matrix argument, respectively.

The time derivative of V_{r1} is

$$\dot{V}_{r1} = \breve{\omega}^T M^* \dot{\breve{\omega}} + \breve{\omega}^T J_{\tilde{\phi}}^T K^* \tilde{\phi} + \frac{1}{2} \breve{\omega}^T \dot{M}^* \breve{\omega} =$$
$$= -\breve{\omega}^T D^* \breve{\omega} + \breve{\omega}^T m_{ext}^* + \frac{1}{2} \breve{\omega}^T (\dot{M}^* - 2C^*) \breve{\omega} =$$
$$= -\breve{\omega}^T D^* \breve{\omega} + \breve{\omega}^T m_{ext}^* \leq -\lambda_{min}(D^*)|\breve{\omega}|^2 + |\breve{\omega}||m_{ext}^*| \quad (41)$$
$$\leq -c_{r1}|\breve{\omega}|^2 + c_{r2}|m_{ext}^*|^2 = -\bar{\gamma}_r(|\breve{\omega}|) + \sigma_{r1}(|m_{ext}^*|)$$

where c_{r1}, c_{r2} = const. > 0. In the computation of the derivative, the relations (36)-(38b) and the property $\breve{\omega}^T(\dot{M}^* - 2C^*)\breve{\omega} = 0$ are used. For the last inequality, note that for all $v, w \in \mathbb{R}$ the inequality $2vw \leq \frac{1}{a}v^2 + aw^2$ is valid, with $a > 0$.

From this result, recalling Definition 3 and considering $y = \breve{\omega}$, it is possible to say that the system admits a qISS-Lyapunov function. Note also that the system is passive w.r.t. the pair $(\breve{\omega}, m_{ext}^*)$.

Now, consider the candidate Lyapunov function V_{r2}, which is defined by slightly modifying V_{r1}:

$$V_{r2} = \frac{1}{2}\breve{\omega}^T M^* \breve{\omega} + \frac{1}{2}\tilde{\phi}^T K^* \tilde{\phi} + \epsilon \frac{\tilde{\phi}^T M^* \breve{\omega}}{\sqrt{1 + \tilde{\phi}^T \tilde{\phi}}}, \quad (42)$$

$$\frac{1}{2}(\lambda_{min}^*(M^*, K^*) - \epsilon\lambda_{max}(M^*))(|\breve{\omega}|^2 + |\tilde{\phi}|^2) \leq V_{r2} \leq \frac{1}{2}(\lambda_{max}^*(M^*, K^*) + \epsilon\lambda_{max}(M^*))(|\breve{\omega}|^2 + |\tilde{\phi}|^2), \quad (43)$$

with the constant ϵ sufficiently small and satisfying $0 < \epsilon < \frac{\lambda_{min}^*(M^*, K^*)}{\lambda_{max}(M^*)}$.

The time derivative of V_{r2} is

$$\dot{V}_{r2} = \breve{\omega}^T M^* \dot{\breve{\omega}} + \breve{\omega}^T J_{\tilde{\phi}}^T K^* \tilde{\phi} + \frac{1}{2}\breve{\omega}^T \dot{M}^* \breve{\omega} + \epsilon\frac{\breve{\omega}^T J_{\tilde{\phi}}^T M^* \breve{\omega}}{\sqrt{1 + \tilde{\phi}^T \tilde{\phi}}} +$$
$$+ \epsilon\frac{\tilde{\phi}^T \dot{M}^* \breve{\omega}}{\sqrt{1 + \tilde{\phi}^T \tilde{\phi}}} + \epsilon\frac{\tilde{\phi}^T M^* \dot{\breve{\omega}}}{\sqrt{1 + \tilde{\phi}^T \tilde{\phi}}} - \epsilon\frac{(\tilde{\phi}^T J_{\tilde{\phi}}\breve{\omega})(\tilde{\phi}^T M^* \breve{\omega})}{(1 + \tilde{\phi}^T \tilde{\phi})^{\frac{3}{2}}} =$$
$$= -\breve{\omega}^T D^* \breve{\omega} - \epsilon\frac{\tilde{\phi}^T J_{\tilde{\phi}}^T K^* \tilde{\phi}}{\sqrt{1 + \tilde{\phi}^T \tilde{\phi}}} + \epsilon\frac{\breve{\omega}^T J_{\tilde{\phi}}^T M^* \breve{\omega}}{\sqrt{1 + \tilde{\phi}^T \tilde{\phi}}} + \quad (44)$$
$$+ \epsilon\frac{\tilde{\phi}^T (\dot{M}^* - C^*)\breve{\omega}}{\sqrt{1 + \tilde{\phi}^T \tilde{\phi}}} - \epsilon\frac{\tilde{\phi}^T D^* \breve{\omega}}{\sqrt{1 + \tilde{\phi}^T \tilde{\phi}}} + \epsilon\frac{\tilde{\phi}^T m_{ext}^*}{\sqrt{1 + \tilde{\phi}^T \tilde{\phi}}} +$$
$$- \epsilon\frac{(\tilde{\phi}^T J_{\tilde{\phi}}\breve{\omega})(\tilde{\phi}^T M^* \breve{\omega})}{(1 + \tilde{\phi}^T \tilde{\phi})^{\frac{3}{2}}} + \breve{\omega}^T m_{ext}^*$$

As previously, the equations (36)-(38b) and the property $\breve{\omega}^T(\dot{M}^* - 2C^*)\breve{\omega} = 0$ are used in the derivation of (44).

In order to find an upper bound for $\dot{V}_{r2}$, the following properties and assumptions are used:

- for all $v, w \in \mathbb{R}$, $2vw \leq \frac{1}{a}v^2 + aw^2$, with $a > 0$;
- only revolute joints are considered, and thus M^* is a periodic function of q. Therefore, $|M^*| \leq d_1$, $|\dot{M}^*| \leq d_2|\breve{\omega}|$,

$|C^*| \le d_3 |\breve{\omega}|$, with $d_1, d_2, d_3 = \text{const.} > 0$ [35];

- it is assumed that $0 < \tilde{\eta} \le 1$;
- all the functions $\dfrac{|\tilde{\phi}|}{\sqrt{1+|\tilde{\phi}|^2}}$, $\dfrac{1}{\sqrt{1+|\tilde{\phi}|^2}}$, $\dfrac{|\tilde{\phi}|}{(1+|\tilde{\phi}|^2)^{\frac{3}{2}}}$ are positive and bounded by 1.

Then, considering one term of (44) at a time, the following relations can be written:

$$
\frac{\tilde{\phi}^T J_{\tilde{\phi}}^T K^* \tilde{\phi}}{\sqrt{1+\tilde{\phi}^T \tilde{\phi}}} = \frac{1}{\sqrt{1+\tilde{\phi}^T \tilde{\phi}}} \begin{bmatrix} 2\tilde{\epsilon}^T & \tilde{q}^T \end{bmatrix} \begin{bmatrix} (\tilde{\eta}E - [\tilde{\epsilon}]^\wedge) & \mathbf{0} \\ \mathbf{0} & E \end{bmatrix} \begin{bmatrix} K_{\tilde{\epsilon}}^* & \mathbf{0} \\ \mathbf{0} & K_{\tilde{q}}^* \end{bmatrix} \begin{bmatrix} 2\tilde{\epsilon} \\ \tilde{q} \end{bmatrix} =
$$

$$
= \frac{1}{\sqrt{1+\tilde{\phi}^T \tilde{\phi}}} \begin{bmatrix} 2\tilde{\epsilon}^T & \tilde{q}^T \end{bmatrix} \begin{bmatrix} \tilde{\eta}K_{\tilde{\epsilon}}^* & \mathbf{0} \\ \mathbf{0} & K_{\tilde{q}}^* \end{bmatrix} \begin{bmatrix} 2\tilde{\epsilon} \\ \tilde{q} \end{bmatrix} = \frac{\tilde{\phi}^T \tilde{K}^* \tilde{\phi}}{\sqrt{1+\tilde{\phi}^T \tilde{\phi}}}, \tag{45}
$$

$$
\epsilon \frac{\breve{\omega}^T J_{\tilde{\phi}}^T M^* \breve{\omega}}{\sqrt{1+\tilde{\phi}^T \tilde{\phi}}} \le \epsilon \frac{|J_{\tilde{\phi}}^T||M^*||\breve{\omega}|^2}{\sqrt{1+|\tilde{\phi}|^2}} \le \epsilon |J_{\tilde{\phi}}^T||M^*||\breve{\omega}|^2 \le a_{r1}|\breve{\omega}|^2, \tag{46}
$$

$$
\epsilon \frac{\tilde{\phi}^T (\dot{M}^* - C^*)\breve{\omega}}{\sqrt{1+\tilde{\phi}^T \tilde{\phi}}} \le \epsilon \frac{|\tilde{\phi}|}{\sqrt{1+|\tilde{\phi}|^2}}(|\dot{M}^*| + |C^*|)|\breve{\omega}|
$$

$$
\le \epsilon(|\dot{M}^*| + |C^*|)|\breve{\omega}| \le a_{r2}|\breve{\omega}|^2, \tag{47}
$$

$$
-\epsilon \frac{\tilde{\phi}^T D^* \breve{\omega}}{\sqrt{1+\tilde{\phi}^T \tilde{\phi}}} \le \epsilon \frac{|D^*||\tilde{\phi}||\breve{\omega}|}{\sqrt{1+|\tilde{\phi}|^2}}
$$

$$
\le \epsilon|D^*||\breve{\omega}| \le a_{r3}|\breve{\omega}|, \tag{48}
$$

$$
-\epsilon \frac{(\tilde{\phi}^T J_{\tilde{\phi}} \breve{\omega})(\tilde{\phi}^T M^* \breve{\omega})}{(1+\tilde{\phi}^T \tilde{\phi})^{\frac{3}{2}}} \le \epsilon \frac{|J_{\tilde{\phi}}||M^*||\tilde{\phi}|^2|\breve{\omega}|^2}{(1+|\tilde{\phi}|^2)^{\frac{3}{2}}}
$$

$$
\le \epsilon|J_{\tilde{\phi}}^T||M^*||\breve{\omega}|^2 \le a_{r1}|\breve{\omega}|^2 \tag{49}
$$

$$
\breve{\omega}^T m_{ext}^* \le |\breve{\omega}||m_{ext}^*| \le c_{r3}|\breve{\omega}|^2 + c_{r2}|m_{ext}^*|^2 \tag{50}
$$

$$
\epsilon \frac{\tilde{\phi}^T m_{ext}^*}{\sqrt{1+\tilde{\phi}^T \tilde{\phi}}} \le \epsilon \frac{|\tilde{\phi}|}{\sqrt{1+|\tilde{\phi}|^2}}|m_{ext}^*| \le \epsilon|m_{ext}^*| \tag{51}
$$

where $a_{r1}, a_{r2}, a_{r3}, c_{r3} = \text{const.} > 0$.

Using Eqs. (45)-(51), it is possible to find an upper bound for the time derivative of V_{r2} as follows:

$$
\begin{aligned}
\dot{V}_{r2} \leq & -\breve{\omega}^T D^* \breve{\omega} - \epsilon \frac{\tilde{\phi}^T \tilde{K}^* \tilde{\phi}}{\sqrt{1 + \tilde{\phi}^T \tilde{\phi}}} + \\
& + (c_{r2}|m_{ext}^*|^2 + \epsilon|m_{ext}^*|) + (c_{r4}|\breve{\omega}|^2 + a_{r3}|\breve{\omega}|) \\
\leq & -\lambda_{min}(D^*)|\breve{\omega}|^2 - \epsilon \lambda_{min}(\tilde{K}^*) \frac{|\tilde{\phi}|^2}{\sqrt{1 + |\tilde{\phi}|^2}} + \\
& + (c_{r2}|m_{ext}^*|^2 + \epsilon|m_{ext}^*|) + (c_{r4}|\breve{\omega}|^2 + a_{r3}|\breve{\omega}|) \\
\leq & -\lambda_{min}^*(D^*, \epsilon\tilde{K}^*) \frac{|\breve{\omega}|^2 + |\tilde{\phi}|^2}{\sqrt{1 + |\breve{\omega}|^2 + |\tilde{\phi}|^2}} + \\
& + (c_{r2}|m_{ext}^*|^2 + \epsilon|m_{ext}^*|) + (c_{r4}|\breve{\omega}|^2 + a_{r3}|\breve{\omega}|) = \\
= & -\gamma_r(|[\tilde{\phi}^T \ \breve{\omega}^T]^T|) + \sigma_{r2}(|m_{ext}^*|) + \lambda_r(|\breve{\omega}|),
\end{aligned}
\tag{52}
$$

where $c_{r4} = 2a_{r1} + a_{r2} = \text{const.} > 0$.

Recalling the Definition 2 and considering $y = \breve{\omega}$, V_{r2} is an IOSS-Lyapunov function for the system (38b). Moreover, $\limsup_{r \to \infty} \lambda_r(r)/\bar{\gamma}_r(r)$ is a constant, and thus the controlled system (38b) is ISS by virtue of the Theorem 1. ∎

Proposition 2: the controlled translational dynamics (38a) of the free-flying orbital robot is input-to-state stable.

Proof. In the following only the main steps are reported since the proof is analogous to the previous one on the attitude-joints dynamics.

Consider the following candidate Lyapunov function:

$$
V_{t1} = \frac{1}{2} m v_c^T v_c + \frac{1}{2} \tilde{x}_c^T K_c \tilde{x}_c,
\tag{53}
$$

$$
\frac{1}{2} \lambda_{min}^*(m, K_c)(|v_c|^2 + |\tilde{x}_c|^2) \leq V_{t1} \leq \frac{1}{2} \lambda_{max}^*(m, K_c)(|v_c|^2 + |\tilde{x}_c|^2).
\tag{54}
$$

The time derivative of V_{t1} is

$$
\begin{aligned}
\dot{V}_{t1} = & v_c^T m \dot{v}_c + v_c^T K_c x_c = -v_c^T D_c v_c + v_c^T f_{ext,t} \\
\leq & -c_{t1}|v_c|^2 + c_{t2}|f_{ext,t}|^2 = -\bar{\gamma}_t(|v_c|) + \sigma_{t1}(|f_{ext,t}|),
\end{aligned}
\tag{55}
$$

where $c_{t1}, c_{t2} = \text{const.} > 0$. Therefore, recalling Definition 3, the controlled system (38a) admits a qISS Lyapunov function. Also in this case, note that the controlled system (38a) is also passive w.r.t. the pair $(v_c, f_{ext,t})$.

Define another candidate Lyapunov function as follows

$$V_{t2} = \frac{1}{2} m \mathbf{v}_c^T \mathbf{v}_c + \frac{1}{2} \tilde{\mathbf{x}}_c^T \mathbf{K}_c \tilde{\mathbf{x}}_c + \epsilon \frac{\tilde{\mathbf{x}}_c^T m \mathbf{v}_c}{\sqrt{1 + \tilde{\mathbf{x}}_c^T \tilde{\mathbf{x}}_c}}, \tag{56}$$

$$\frac{1}{2} (\lambda_{min}^*(m, \mathbf{K}_c) - \epsilon m)(|\mathbf{v}_c|^2 + |\tilde{\mathbf{x}}_c|^2) \le V_{t2} \le \frac{1}{2} (\lambda_{max}^*(m, \mathbf{K}_c) + \epsilon m)(|\mathbf{v}_c|^2 + |\tilde{\mathbf{x}}_c|^2), \tag{57}$$

with the constant ϵ sufficiently small and satisfying $0 < \epsilon < \frac{\lambda_{min}^*(m, \mathbf{K}_c)}{m}$.

The time derivative of V_{t2} can be computed as follows

$$\begin{aligned}
\dot{V}_{t2} =& \mathbf{v}_c^T m \dot{\mathbf{v}}_c + \mathbf{v}_c^T \mathbf{K}_c \mathbf{x}_c + \epsilon \frac{\mathbf{v}_c^T m \mathbf{v}_c}{\sqrt{1 + \tilde{\mathbf{x}}_c^T \tilde{\mathbf{x}}_c}} + \\
&+ \epsilon \frac{\tilde{\mathbf{x}}_c^T m \dot{\mathbf{v}}_c}{\sqrt{1 + \tilde{\mathbf{x}}_c^T \tilde{\mathbf{x}}_c}} + \epsilon \frac{(\mathbf{x}_c^T \mathbf{v}_c)(\mathbf{x}_c^T m \mathbf{v}_c)}{(1 + \tilde{\mathbf{x}}_c^T \tilde{\mathbf{x}}_c)^{\frac{3}{2}}} = \\
=& - \mathbf{v}_c^T \mathbf{D}_c \mathbf{v}_c + \mathbf{v}_c^T \mathbf{f}_{ext,t} + \epsilon \frac{\mathbf{v}_c^T m \mathbf{v}_c}{\sqrt{1 + \tilde{\mathbf{x}}_c^T \tilde{\mathbf{x}}_c}} + \\
&- \epsilon \frac{\tilde{\mathbf{x}}_c^T \mathbf{D}_c \mathbf{v}_c}{\sqrt{1 + \tilde{\mathbf{x}}_c^T \tilde{\mathbf{x}}_c}} - \epsilon \frac{\tilde{\mathbf{x}}_c^T \mathbf{K}_c \tilde{\mathbf{x}}_c}{\sqrt{1 + \tilde{\mathbf{x}}_c^T \tilde{\mathbf{x}}_c}} + \\
&+ \epsilon \frac{\tilde{\mathbf{x}}_c^T \mathbf{f}_{ext,t}}{\sqrt{1 + \tilde{\mathbf{x}}_c^T \tilde{\mathbf{x}}_c}} + \epsilon \frac{(\mathbf{x}_c^T \mathbf{v}_c)(\mathbf{x}_c^T m \mathbf{v}_c)}{(1 + \tilde{\mathbf{x}}_c^T \tilde{\mathbf{x}}_c)^{\frac{3}{2}}} \\
\le& - \mathbf{v}_c^T \mathbf{D}_c \mathbf{v}_c - \epsilon \frac{\tilde{\mathbf{x}}_c^T \mathbf{K}_c \tilde{\mathbf{x}}_c}{\sqrt{1 + \tilde{\mathbf{x}}_c^T \tilde{\mathbf{x}}_c}} + \mathbf{v}_c^T \mathbf{f}_{ext,t} + \\
&+ (2a_{t1} |\mathbf{v}_c|^2 + a_{t3} |\mathbf{v}_c|) + \epsilon |\mathbf{f}_{ext,t}| \\
\le& - \lambda_{min}^*(\mathbf{D}_c, \epsilon \mathbf{K}_c) \frac{|\mathbf{v}_c|^2 + |\tilde{\mathbf{x}}_c|^2}{\sqrt{1 + |\mathbf{v}_c|^2 + |\tilde{\mathbf{x}}_c|^2}} + \\
&+ (c_{t4} |\mathbf{v}_c|^2 + a_{t3} |\mathbf{v}_c|) + (c_{t2} |\mathbf{f}_{ext,t}|^2 + \epsilon |\mathbf{f}_{ext,t}|) = \\
=& - \gamma_t ([\tilde{\mathbf{x}}_c^T \ \mathbf{v}_c^T]^T) + \sigma_{t2}(|\mathbf{f}_{ext,t}|) + \lambda_t(|\mathbf{v}_c|),
\end{aligned} \tag{58}$$

where $a_{t1}, a_{t3}, c_{t4} = $ const. > 0.

Recalling Definition 2, the controlled system (38a) is said to admit an IOSS Lyapunov function. Since $\limsup_{r \to \infty} \lambda_t(r)/\bar{\gamma}_t(r)$ is a constant, it is possible to conclude that also the system (38a) is ISS by virtue of Theorem 1. ∎

C. Reaction setpoints

As already explained, the spacecraft is commanded to a desired attitude, while the manipulator is moving and the entire robot is translating away from the obstacle. To this aim, the information from the observer can be used in order to identify the escape direction. Indeed, the desired position of the center of mass $\mathbf{p}_{tc,d} \in \mathbb{R}^3$ and of the joints $\mathbf{q}_d \in \mathbb{R}^n$

can be defined as follows:

$$p_{tc,d} = p_{tc,td} + \Delta_{p_{tc}} \frac{\hat{f}_{ext,t}}{|\hat{f}_{ext,t}|}, \tag{59}$$

$$q_d = q_{td} + \Delta_q \frac{\hat{\tau}_{ext}}{|\hat{\tau}_{ext}|}, \tag{60}$$

where

$$\hat{\tau}_{ext} = \hat{\tau}^*_{ext} + \bar{J}_v^T R_{tb}^T \hat{f}_{ext,t} \in \mathbb{R}^n, \tag{61}$$

and where $p_{tc,td} \in \mathbb{R}^3$, $q_{td} \in \mathbb{R}^n$ are the CoM position and joint positions at the detected contact time, respectively, and $\Delta_{p_{tc}}, \Delta_q \in \mathbb{R}$ are some desired constant "bounce" coefficients, which define the amount of displacement. Thanks to the second term in both Eqs. (59) and (60), the robot is commanded to move along the direction of the external contact force, projected in the frame $\mathcal{T}$ and in the joints space, respectively, escaping from the obstacle. In order to perform this maneuver, an estimate of the actual joint contact torques is necessary since it provides directly the escape direction at the joint level. This estimate can be obtained through Eq. (61). Note that the estimate $\hat{f}_{ext,t}$ can be derived multiplying the force in the reconstructed wrench (25) by R_{tp}. The parameters $\Delta_{p_{tc}}, \Delta_q$ should be selected depending on the scenario. In particular, an assessment of a safe distance should be performed depending on the mission, the geometry of the target and the presence of other objects close to each other. The "bounce" coefficients can also be set equal to zero. In this case, the robot would stop keeping the position and configuration at the detection time. For instance, in some situations with the collision at arm level, it could be convenient for the operations to move away from the obstacle only with the manipulator, while keeping the position of the CoM.

D. Discussion on the proposed control strategy

In the proposed control strategy, the space robot system is like split into an "external" translational motion of the entire composite body and an "internal" rotational motion modifying the configuration. The spacecraft force actuators are used to move the center of mass of the whole system, and their action is compensated at the attitude and joint level thanks to the triangular form of the Eq. (11). This can be seen imaging to impose a change in the position of the CoM, and setting m_c and τ^* to zero. When the computed control actions are transformed into the real ones provided by the actuators through Eq. (11), all the actuators are activated. In particular, the base force is used to translate the CoM of the whole system, while the base torque and the joint torques are used to keep the position compensating the disturbance caused by the translation.

The proposed controller is developed only to address the reaction to an unexpected collision. However, it could be used for the nominal operations as well, such as reaching a target. In this case, note that the translational control is activated only when an external contact occurs, modifying the position of the CoM, while in the contact-free phase only

attitude and joint positions are controlled. This means that, in case the attitude is actuated only through momentum exchange devices, the use of the thrusters can be completely avoided. In contrast, when the thrusters are employed also to actuate the attitude, the fuel consumption is reduced. However, for the nominal operations, it would be better to control the manipulator in the operational space, instead of the joints space. To this aim, a controller similar to the one presented herein was proposed recently in [29] by one of the author, which is based on this transformation:

$$
\begin{bmatrix} \boldsymbol{v}_c \\ \boldsymbol{\omega}_b \\ \boldsymbol{v}_e^{\oplus} \end{bmatrix} = \begin{bmatrix} \boldsymbol{R}_{tb} & -\boldsymbol{R}_{tb}[\boldsymbol{p}_{bc}]^{\wedge} & \boldsymbol{R}_{tb}\bar{\boldsymbol{J}}_v \\ \boldsymbol{0} & \boldsymbol{E} & \boldsymbol{0} \\ \boldsymbol{0} & \boldsymbol{G}_{\omega_b} & \boldsymbol{J}_{v_e}^{\oplus} \end{bmatrix} \begin{bmatrix} \boldsymbol{v}_b \\ \boldsymbol{\omega}_b \\ \dot{\boldsymbol{q}} \end{bmatrix},
\tag{62}
$$

where

$$
\boldsymbol{v}_e^{\oplus} = \boldsymbol{v}_e - \begin{bmatrix} \boldsymbol{R}_{et} \\ \boldsymbol{0} \end{bmatrix} \boldsymbol{v}_c
\tag{63}
$$

and where $\boldsymbol{v}_e^{\oplus} \in \mathbb{R}^6$ is called "end-effector circumcentroidal motion", i.e., the motion around the CoM, $\boldsymbol{G}_{\omega_b} \in \mathbb{R}^{6 \times 3}$ and $\boldsymbol{J}_{v_e}^{\oplus} \in \mathbb{R}^{6 \times n}$ are matrices mapping the angular velocity of the spacecraft and the joints in the circumcentroidal motion. The vector $\boldsymbol{v}_e^{\oplus}$ is exactly equal to the vector containing the linear and angular velocity of the end-effector, $\boldsymbol{v}_e \in \mathbb{R}^6$, when the velocity of the CoM of the whole system is zero. More detail about this controller can be found in [29].

The main difference between the strategy in [29] and the one proposed here is exactly the control of the manipulator, that in [29] is controlled in the end-effector space, whereas the present controller works in joint space. Note that these two controllers can actually work together since they address two different objectives. The space robot can be controlled by the strategy in [29] during the nominal operations, which require end-effector maneuvering. When an unexpected collision occurs, which does not satisfy safety criteria, the robot switches to the control proposed in this paper, limiting the possible damages. For the reaction phase, it is better to control the system in the joints space since the manipulator can be controlled without taking care of possible singular configurations or degrees of freedom in the end-effector's null space (in case of redundant arm). Indeed, the goal of the reaction phase is to move the robot safely and quickly in a configuration and position away from the obstacle, and this can be achieved efficiently by the proposed controller.

The integration of these two controllers leads to a control system capable of operating in both nominal and emergency conditions, and saving fuel in contact-free end-effector maneuvering. The switch between the controllers occurs in case of a risky situation and just at the manipulator control level. Only when the robot is safe, the control is switched back. In the simulation example presented later in the paper, the performance of the proposed controller is assessed imaging a scenario in which a nominal operation is performed using the controller in [29] and at a certain time the robot switches the control to face an unplanned collision.
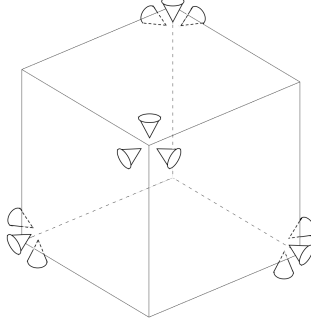
Fig. 3   Position of the thrusters on the spacecraft.

E. VSCMG integration

In this paper, it is assumed that the actuation system of the spacecraft comprises a set of 12 thrusters and 4 variable speed control moment gyros (VSCMG) in a pyramid configuration. The position of the thrusters is reported in Fig. 3. The commanded base force, computed by Eqs. (11) and (35a), is modulated through a pulse width modulation (PWM) approach and provided directly to the thrusters. The commanded base torque is actuated by the VSCMG, as analyzed in more detail in the following.

Consider a reference frame attached to each VSCMG and defined by the following three versors:

- $\hat{\boldsymbol{n}}_s$ is the spin axis, along the rotation axis of the wheel;
- $\hat{\boldsymbol{n}}_g$ is the gimbal axis, along the rotation axis of the gimbal;
- $\hat{\boldsymbol{n}}_t$ is the axis that completes the frame $\{\hat{\boldsymbol{n}}_s, \hat{\boldsymbol{n}}_t, \hat{\boldsymbol{n}}_g\}$.

The equations of motion for a spacecraft with a cluster of k VSCMG have been developed in [36], and the angular momentum of the spacecraft-VSCMG ensemble, expressed in $\mathcal{B}$, is

$$\boldsymbol{h}^r_{b,\Omega} = \boldsymbol{I}_{b,\Omega}\boldsymbol{\omega}_b + \underbrace{\boldsymbol{U}_g \boldsymbol{I}_{cg}\dot{\boldsymbol{\gamma}} + \boldsymbol{U}_s \boldsymbol{I}_{ws}\boldsymbol{\omega}_w}_{\boldsymbol{h}_\Omega \in \mathbb{R}^3} \in \mathbb{R}^3, \tag{64}$$

where $\boldsymbol{U}_g$, $\boldsymbol{U}_s \in \mathbb{R}^{3\times k}$ are matrices having as columns the directions of the gimbal and spin directional unit vectors, respectively, expressed in the frame $\mathcal{B}$, $\boldsymbol{I}_{cg} \in \mathbb{R}^{k\times k}$ is a diagonal matrix having as elements the inertias along the axes $\hat{\boldsymbol{n}}_g$ of the gimbal-wheel structures, $\boldsymbol{I}_{ws} \in \mathbb{R}^{k\times k}$ is a diagonal matrix having as elements the inertias along the axes $\hat{\boldsymbol{n}}_s$ of the only-wheel structures, $\dot{\boldsymbol{\gamma}}$, $\boldsymbol{\omega}_w \in \mathbb{R}^k$ are the vector of the gimbal angular velocities and the vector of the wheel angular velocities, respectively, both expressed in the VSCMG frame, $\boldsymbol{h}_\Omega$ is the contribution of the VSCMG to the angular momentum of the spacecraft-VSCMG ensemble, and $\boldsymbol{I}_{b,\Omega} \in \mathbb{R}^{3\times 3}$ is defined as

$$\boldsymbol{I}_{b,\Omega} = \boldsymbol{I}_b + \boldsymbol{U}_s \boldsymbol{I}_{cs}\boldsymbol{U}_s^T + \boldsymbol{U}_t \boldsymbol{I}_{ct}\boldsymbol{U}_t^T + \boldsymbol{U}_g \boldsymbol{I}_{cg}\boldsymbol{U}_g^T, \tag{65}$$

where $I_b \in \mathbb{R}^{3\times3}$ is the inertia matrix of the spacecraft including the point masses of the VSCMG, I_{ct}, $I_{cs} \in \mathbb{R}^{k\times k}$ are diagonal matrices having as elements the inertias along the axes $\hat{n}_t$ and $\hat{n}_s$ of the gimbal-wheel structures, respectively, and $U_t \in \mathbb{R}^{3\times k}$ is a matrix having as columns the directions of the transverse directional unit vectors, expressed in the frame $\mathcal{B}$.

Computing the time derivative of Eq. (64), it is possible to find the relation between the actuation torque m_b and the control parameters $\dot{\gamma}$ and $\dot{\omega}_w$ [37]:

$$m_b = -\dot{I}_{b,\Omega}\omega_b - \dot{h}_\Omega - [\omega_b]^\wedge h_\Omega. \tag{66}$$

Typically, the gimbal acceleration term in $\dot{h}_\Omega$ can be neglected, and the control parameters can be computed as [37]

$$\begin{bmatrix} \dot{\gamma} \\ \\ \dot{\omega}_w \end{bmatrix} = -G^\#(m_b + [\omega_b]^\wedge U_s I_{ws}\omega_w), \tag{67}$$

where

$$G = \begin{bmatrix} C & D \end{bmatrix} \in \mathbb{R}^{3\times 2k}, \tag{68}$$

$$C = W + U_t I_{ws}[\omega_w]^d + [\omega_b]^\wedge U_g I_{cg} \in \mathbb{R}^{3\times k}, \tag{69}$$

$$D = U_s I_{ws} \in \mathbb{R}^{3\times k}, \tag{70}$$

$$W = U_t(I_{cs} - I_{ct})[U_s^T \omega_b]^d + U_s(I_{cs} - I_{ct})[U_t^T \omega_b]^d \in \mathbb{R}^{3\times k}, \tag{71}$$

and where the operator $[\,\cdot\,]^d$ stands for a diagonal matrix with its elements being the components of the argument vector.

Introducing the VSCMG, it is necessary to include their contribution to the momentum in the computation of the angular momentum residual in order to estimate correctly the contact torque. To this aim, the Eq. (20b) can be modified in the following way:

$$\hat{m}_{ext,c} = K_m\left(h_{c,\Omega}^r - \int_0^t (-[p_{bc}]^\wedge f_b - [\omega_b]^\wedge h_{c,\Omega}^r + \hat{m}_{ext,c})ds\right), \tag{72}$$

where

$$h_{c,\Omega}^r = I_{c,\Omega}\omega_b + I_{c,\Omega}\bar{J}_\omega\dot{q} + U_g I_{cg}\dot{\gamma} + U_s I_{ws}\omega_w \in \mathbb{R}^3, \tag{73}$$

and where $I_{c,\Omega} \in \mathbb{R}^{3\times3}$ is the rotational inertia around C including the VSCMG contribution. Also in this case, it can be proved that $\hat{m}_{ext,c}$ is the first-order-filtered estimation of $m_{ext,c}$.

The new definition of the angular momentum residual (72) is valid for any momentum exchange devices. Indeed, if the reaction wheels are selected, it is sufficient to set $\dot{\gamma} = 0$; if the control moment gyros are chosen, ω_w will be

constant; finally, if the VSCMG are preferred, as in this study, both $\dot{\gamma}$ and ω_w can vary in time.

As last remark, note that the ISS stability proof developed in Sect. V.B does not consider the dynamics of the actuators. Its inclusion in the stability analysis is left for future work.

VI. Simulation example

A. Simulation scenario and setup

A spacecraft mounting a 7DoF robotic arm is considered. The kinematics and dynamics parameters are reported in Tab. 1. As already said, the spacecraft is equipped with 4 variable speed control moment gyros in a pyramid configuration and 12 thrusters, commanded through a PWM approach. In order to have a realistic simulation scenario, the model of the thrusters includes a delay in the activation, due to the opening/closure of the valve, a dead-zone and a first-order dynamics with different time constant for the rising and falling phase. Therefore, the controller commands a certain action, but the system receives a slightly different one. The characteristics of both actuators are reported in Tab. 2, where the parameters f_{max} is the maximum force provided by a single thruster, T_{pwm} is the PWM period, t_{delay} is the delay of the opening/closure of the valve, T_{rising} and $T_{falling}$ are the time constants of the first-order dynamics. The spacecraft is endowed with an IMU, measuring accelerations and angular velocities, a star tracker for the attitude, a vision system for measuring the relative distance, while the manipulator's joints position and torques are measured by encoders and torque sensors, respectively. The noise model for the measurements is presented in the following section.

For the translational and attitude control, the gains are the same for x, y and z directions: $k_c = 100$ Nm^{-1} and $d_c = 250$ Ns, $k_{\tilde{\epsilon}} = 750$ Nmrad^{-1} and $d_{\omega_b} = 300$ Nmsrad^{-1}. For the first four joints, the gains $k_{\tilde{q}} = 70$ Nmrad^{-1} and $d_{\tilde{q}} = 10.5$ Nmsrad^{-1} are set, while for the first two wrist joints, $k_{\tilde{q}} = 1$ Nmrad^{-1} and $d_{\tilde{q}} = 0.7$ Nmsrad^{-1}, and for the last wrist joint $k_{\tilde{q}} = 0.2$ Nmrad^{-1} and $d_{\tilde{q}} = 0.04$ Nmsrad^{-1}. The parameters $\Delta_{p_{tc}}$ and Δ_q are set equal to 0.60 m and 0.26 rad. Finally, the gains for the computation of the residuals $\hat{m}_{ext,c}$ and $\hat{\tau}_{ext}^*$ are set equal to 20 s^{-1}.

The presented multibody dynamics simulations are performed in *Dymola*, which is a commercial software for

Table 1   Kinematics and dynamics parameters.

	l [m]	m [kg]	I_x [kgm^2]	I_y [kgm^2]	I_z [kgm^2]
Base	1.2	150	15	21.8	18.8
Link 1	0.2	2.71	0.023	0.023	0.005
Link 2	0.2	2.71	0.026	0.026	0.053
Link 3	0.2	2.54	0.014	0.014	0.005
Link 4	0.2	2.50	0.028	0.028	0.005
Link 5	0.19	1.30	0.026	0.026	0.026
Link 6	0.12	1.57	0.003	0.003	0.003
Link 7	0	0.2	0.003	0.003	0.003

Table 2   Actuators parameters.

	Parameters		
VSCMG	$I_{ws} = 0.042\text{kgm}^2$	$I_{wt} = 0.024\text{kgm}^2$	$I_{wg} = 0.024\text{kgm}^2$
	$I_{gs} = 0.093\text{kgm}^2$	$I_{gt} = 0.054\text{kgm}^2$	$I_{gg} = 0.054\text{kgm}^2$
Thrusters	$f_{max} = 4$ N	$T_{pwm} = 50$ ms	$t_{delay} = 8$ ms
	$T_{rising} = 1.5$ ms	$T_{falling} = 3$ ms	

simulation of multi-disciplinary complex systems[‡]. In section VI.C.2, in order to simulate the contact, the *Dymola* library presented in [38] is used. The normal force to the contact surface is modeled as the sum of an elastic and damping terms, which depend on the penetration in the normal direction and, for the damping, its time derivative. Friction is neglected, and thus tangential components are null. Further details can be found in [38].

The dynamic matrices required by the observer (20) are computed through the algorithms proposed in [39].

B. Measurement model and velocity reconstruction

The angular velocity, the joint angles and the joint torques can be directly measured using a gyro, encoders and joint torque sensors, respectively. On the other hand, the linear velocity and the joint velocities are not directly measured but need to be reconstructed, either using a discrete derivative or by data fusion. Herein only the problem of the estimation of the linear velocity is addressed, while a simplified noise performance model is used for the joint velocities.

The measurements of the angular velocity, joint angles and joint velocities are assumed to be affected by a white Gaussian noise with zero mean, while an uniform noise is considered for the torque sensors. For the angular velocity a bias is also introduced leading to the following model [40]:

$$\omega_b^m = \omega_b + \boldsymbol{b}_\omega + \boldsymbol{\eta}_\omega,$$
$$\dot{\boldsymbol{b}}_\omega = \boldsymbol{\eta}_{b\omega},$$
(74)

where $\omega_b^m \in \mathbb{R}^3$ is the measured angular velocity of the base; the term $\boldsymbol{b}_\omega \in \mathbb{R}^3$ is the bias, considered to be a "Brownian" motion process; the terms $\boldsymbol{\eta}_\omega, \boldsymbol{\eta}_{b\omega} \in \mathbb{R}^3$ are white Gaussian noise with zero mean.

The linear velocity is reconstructed through a kinematics-based Kalman filter using a gyro and an accelerometer in the prediction step, and camera measurements for the update step. These sensors are placed on the spacecraft. The camera measures the base position with respect to the inertial frame $\mathcal{T}$ (see Fig. 1), that can be imagined to be located on a target object [41].

The position of the target with respect to the base $\boldsymbol{p}_{bt} \in \mathbb{R}^3$ and base velocity $\boldsymbol{v}_b$, expressed in $\mathcal{B}$, compose the state vector, and their time derivatives are

---

[‡]https://www.3ds.com/products-services/catia/products/dymola

Table 3   Standard deviations and biases of the considered noise model.

σ_q [rad]	$\sigma_{\dot{q}}$ [rad/s]	σ_τ [Nm]	$\sigma_{p_{bt}}$ [m]	$\sigma_{b\omega}$ [μrad/s$^{3/2}$]
$5 \cdot 10^{-5}$	10^{-4}	0.2	0.005	$3.162 \cdot 10^{-4}$

σ_ω [μrad/s$^{1/2}$]	σ_{ba} [m/s$^{5/2}$]	σ_a [m/s$^{3/2}$]	$b_{\omega,0}$ [rad/hr]	$b_{a,0}$ [m/s^2]
0.316	$6.00 \cdot 10^{-5}$	$9.81 \cdot 10^{-5}$	0.0017	0.003

$$\dot{\boldsymbol{p}}_{bt} = -[\boldsymbol{\omega}_b]^\wedge \boldsymbol{p}_{bt} - \boldsymbol{v}_b,$$

$$\dot{\boldsymbol{v}}_b = -[\boldsymbol{\omega}_b]^\wedge \boldsymbol{v}_b + \boldsymbol{a}_b, \tag{75}$$

where $\boldsymbol{a}_b \in \mathbb{R}^3$ is the spacecraft acceleration. Eq. (75) is the prediction step of the filter, where $\boldsymbol{\omega}_b$ and $\boldsymbol{a}_b$ are measured by the inertial measurement unit (IMU), including the gyro and the accelerometer.

The measurement equation is

$$\tilde{\boldsymbol{p}}_{bt} = \boldsymbol{p}_{bt}, \tag{76}$$

where $\tilde{\boldsymbol{p}}_{bt} \in \mathbb{R}^3$ is the measurement vector.

Also for the accelerometer, the noise model (74) is used[42]. On the other hand, for the camera, the noise is introduced by adopting the exponentially correlated random variable model[43][44]

$$\epsilon_{k+1} = K\epsilon_k + \sqrt{1 - K^2}\mathcal{N}(0, \sigma),$$

$$K = e^{-1/(f_a T)}, \tag{77}$$

where ϵ is the error with respect to the true quantity, $\mathcal{N}(0, \sigma)$ is a random number generated with a normal distribution of zero mean and standard deviation σ, f_a is the acquisition frequency and T is the autocorrelation time.

The standard deviations and biases of the considered noise models are reported in Tab. 3. The vision system acquires measurements at 3 Hz, while the other sensors work at 200 Hz. The filter prediction step is performed at 200 Hz, whereas the update step at 3 Hz. Note that the attitude is controlled to be fixed. To achieve this goal, attitude measurements are necessary, and thus it is assumed that the spacecraft is equipped with a star tracker, which measures the Euler angles $\boldsymbol{\Phi} \in \mathbb{R}^3$. The exponentially correlated random variable model reported in Eq. (77) is used to reproduce the noise of the sensor[43], with standard deviation $\sigma_\Phi = 1.04 \cdot 10^{-4}$ rad. The star tracker works at 3 Hz, while the controller works at 200 Hz. Hence, the EKF for quaternions presented in [45] is implemented[§]. Similar to the filter for the base velocity, the prediction step run at 200 Hz, while the update at 3 Hz.

[§]In [45] the filter estimates also the angular velocity and the measurements are assumed to be acquired by a laser vision system. In this work, only the attitude is estimated and the measurements are provided by the star tracker, but the implementation of the filter is analogous.
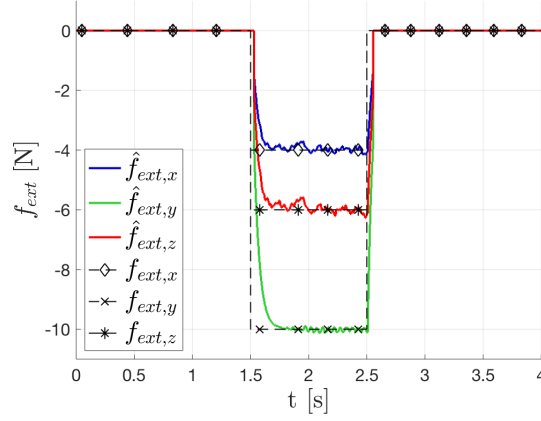
Fig. 4 Reconstruction of the external force acting on a generic point on link 5.

C. Results

1. Observer

Before presenting the results for the complete collision handling, a numerical validation of the observer is presented. In this example, the robot is commanded to keep the initial position of the CoM, attitude and arm configuration through the control (35). At time instant $t = 1.5$ s, a constant force $\boldsymbol{f}_{ext} = [-4 \ -10 \ -6]^T$ N is introduced on a point at the midsection of link 5 for 1 second.

After the detection through the monitoring signals $\hat{\boldsymbol{m}}_{ext,c}$ and $\hat{\boldsymbol{\tau}}_{ext}^*$, the contact is isolated with a maximum error norm of 1.4 cm, which is acceptable for a good reconstruction of the force. The isolation is performed following the scheme shown in Fig. 2. Then, the contact force $\boldsymbol{f}_{ext}$ is estimated through the Eq. (25) and the result is reported in Fig. 4. It can be appreciated that the proposed method based on the observer (20) provides a good estimate of the force acting on a generic point along the robot even in presence of nonidealities, such as sensors noise, thrusters' valve delay and non-modelled dynamics.

2. Collision handling

Initially, the controller presented in [29] is active. The free-flying orbital robot is commanded to keep the initial attitude and position of the CoM. The end-effector is controlled to follow a trapezoidal velocity profile along the y direction, while keeping the initial orientation and initial position along x and z. At a certain time instant, the link 5 of the manipulator collides with another object. See Fig. 5 for a graphical representation of the collision location on the orbital robot. The residuals $\hat{\boldsymbol{m}}_{ext,c}$ and $\hat{\bar{\boldsymbol{\tau}}}_{ext}^*$ are exploited to detect the collision and trigger the reaction control (35). The new setpoints for the joint positions and the CoM position are set through Eqs. (59)-(60), while the attitude is kept.

In Fig. 6, the force generated in the collision is reported in the case in which the reaction control is activated and in the case in which it is not. When the contact occurs, the magnitude of the force is very similar in both situations.

28
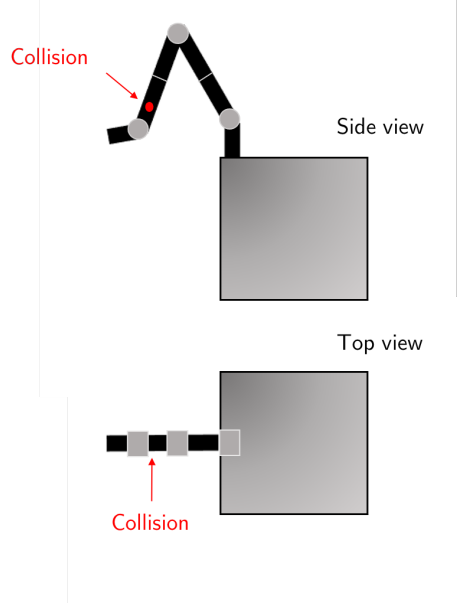
Fig. 5   Graphical representation of the collision location on the robot.

However, in the latter one, the space robot does not recognize the contact and tries to pursue the first goal, namely to move the end-effector along the direction y. Consequently, multiple contacts and the build-up of the force occur. This is a dangerous condition when colliding at high velocity, or with fragile objects, causing serious damages and jeopardizing the mission. On the other hand, if the proposed reaction control is activated, the contact is detected and the robot moves away avoiding other collisions and the increase of the force. In this way, the possible damages are mitigated and the space robot can reach a safe position, where then the subsequent actions can be planned. It is important to stress that this is a capability a space robot should have in order to carry out the mission safely.

Figs. 7a-7b show the residuals $\hat{\boldsymbol{m}}_{ext,c}$ and $\hat{\boldsymbol{\tau}}_{ext}^*$, and the set thresholds for the detection (red dashed lines). The contact is detected both at the angular momentum level and at the joint level. In particular, the contact is recognized on the components x and z of $\hat{\boldsymbol{m}}_{ext,c}$ and by the monitoring signals at the joints 1 and 3. In Fig. 8, the effects of the discrepancy between the commanded thrusters' force and the real one, which includes delay, dead-zone and first-order dynamics, on the residual computation can be noted. Note that this discrepancy, along with other uncertainties and measurements noise, affects the selection of the threshold, and thus the sensitivity. The amplitude of these oscillations can be modified acting on the observer gains.

In Fig. 9, the position of the CoM of the whole system is reported. Until the contact occurs, the position is constant, then the reaction control is activated and the entire spacecraft-manipulator system translates away from the obstacle reaching the new setpoint. Note that the setpoint is computed using Eq. (59), where the external force is estimated through Eq. (25), and the direction of the motion after the contact is along the line of action of the force (see Fig. 6). Indeed, the "bounce" is mainly along the y direction, which is the component of the contact force having
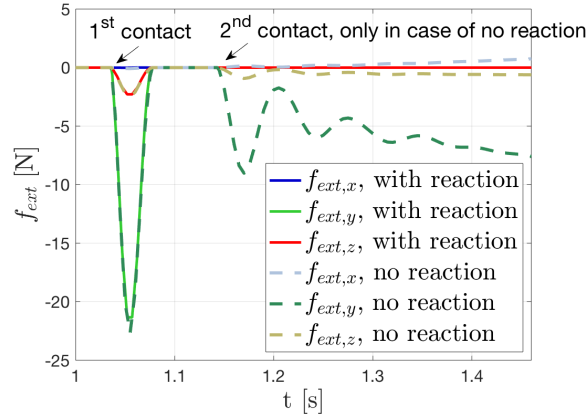
Fig. 6   Contact force generated by the collision in case the reaction control is active and in case it is not.

the higher magnitude in modulus. For the reconstruction, the knowledge of the contact point is necessary and it is performed following the scheme reported in Fig. 2. Therefore, in the simulation, the complete loop detection, isolation, identification and reaction is implemented and was demonstrated to work satisfactorily.

The error on the absolute angles of the spacecraft is reported in Fig. 10. The error is always small, even during the contact phase, and it further decreases after the contact. Note that keeping or moving to a certain fixed orientation can be required either to communicate or to have the target in the field of view of some sensors, e.g. vision system. Finally, Fig. 11 reports the response of the joint angles. Before the contact, the manipulator moves towards the obstacle, following the desired trajectory imposed in the end-effector space. Afterwards, the collision occurred and the new desired positions for the joints are computed by Eq. (60). Smooth trajectories are generated and the manipulator escapes from the obstacle successfully. In particular, joints 1 and 3 mainly contribute to the inversion of the motion. Indeed, higher disturbance torques act on these joints. On the other hand, the last two joints keep basically the same position they have at the contact time. This is because the contact is at link 5, and thus the corresponding components of τ_{ext} are zero, theoretically. Actually, they are not exactly zero in the estimate $\hat{\tau}_{ext}$ due to noise and uncertainties, but very close to zero.
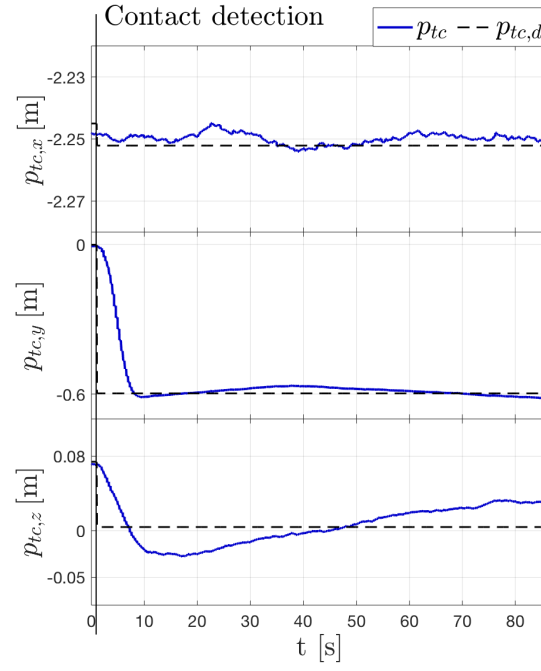
(a) Residual $\hat{\boldsymbol{m}}_{ext,c}$.

(b) Residual $\hat{\bar{\boldsymbol{\tau}}}^*_{ext}$.
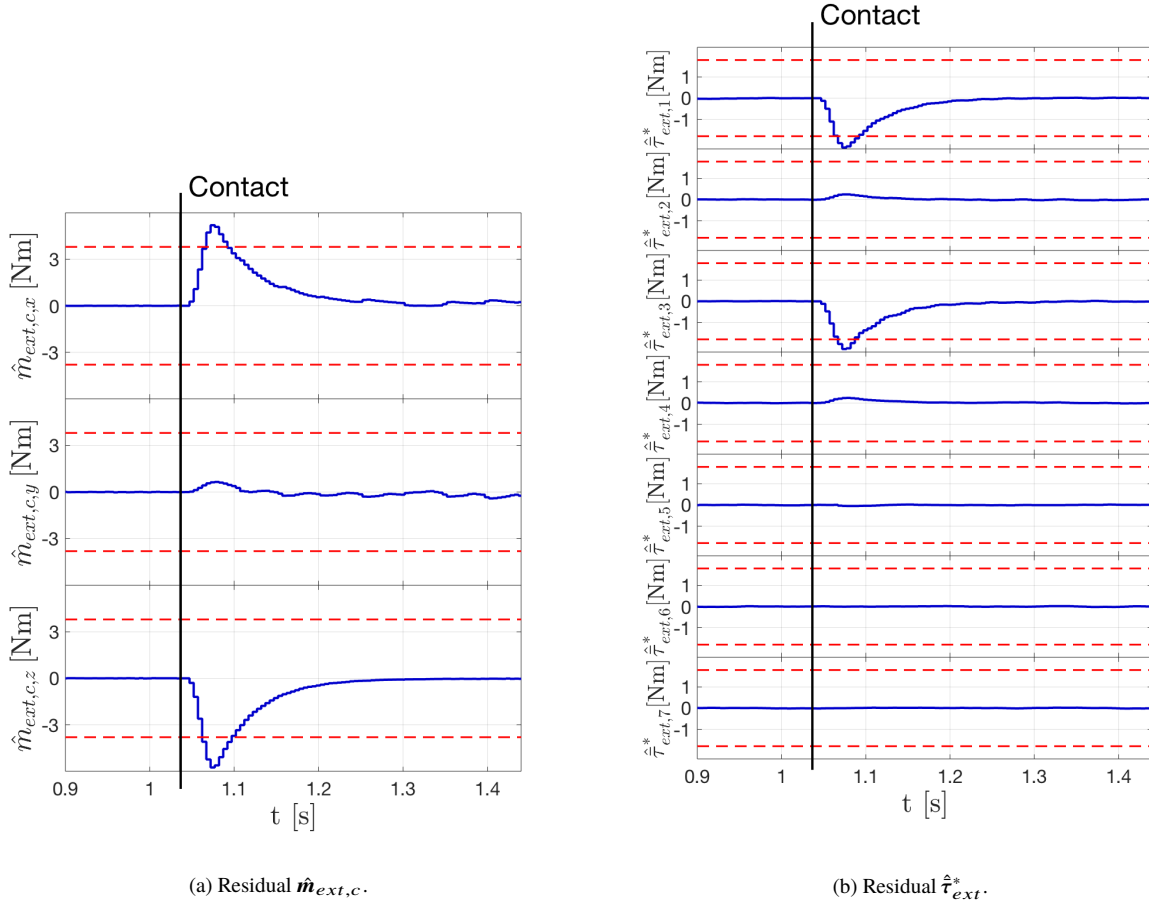
Fig. 7   Components of the residual $\hat{\boldsymbol{m}}_{ext,c}$ and $\hat{\bar{\boldsymbol{\tau}}}^*_{ext}$, and the set thresholds (red dashed line).
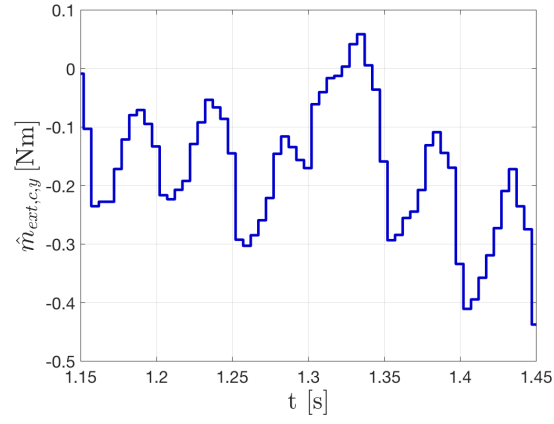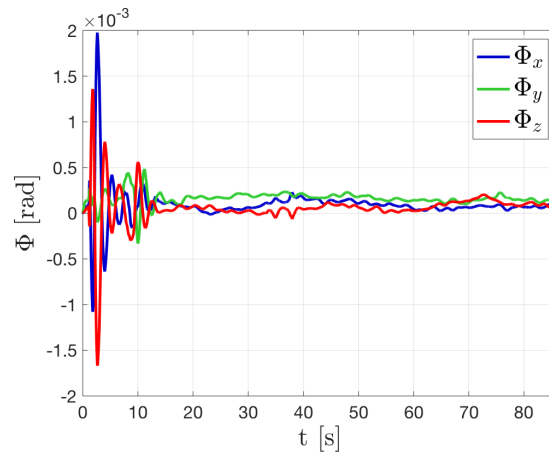

Fig. 8   Effects of the non-modelled dynamics of the thrusters on the residual $\hat{\boldsymbol{m}}_{ext,c}$.
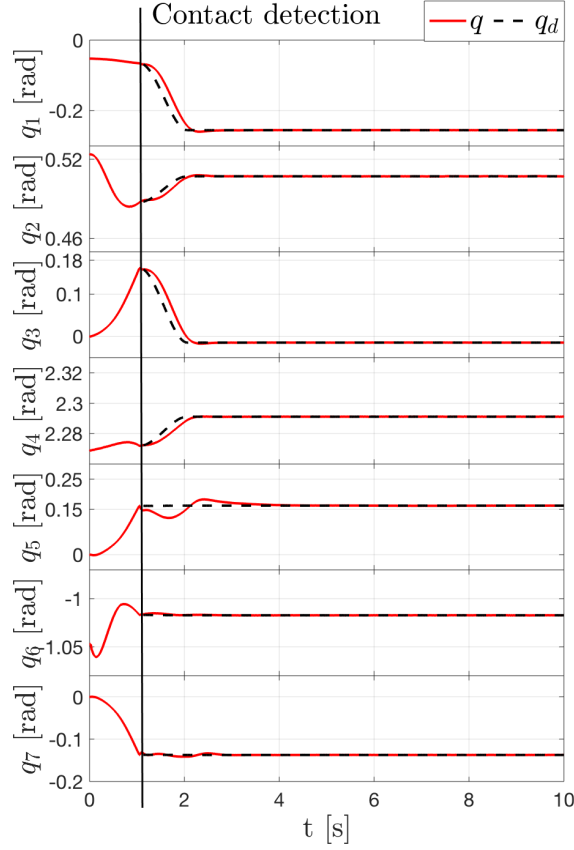
Fig. 9   Response of the CoM position before and after the contact.

Fig. 10   Error on the Euler angles of the spacecraft.

Fig. 11   Response of the position of the joints before and after the contact.

VII. Limitations of the proposed strategy

The proposed reaction strategy is based on the assumption that only one contact occurs at a time. However, dealing with multiple contacts may be necessary, especially in case a grasping operation is planned. In this situation, a contact is expected at the end-effector, and an unexpected collision could occur on another part of the robot at the same time. To face this scenario, the robot could be equipped with a force/torque sensor at the wrist to deal with the planned contact, while the observer is used to detect the unexpected collision. In particular, the sensor measures directly the wrench exchanged between the end-effector and the target, and this information is provided to the model-based observer. The contributions at force, moment and torque level are added in the term under the integral in Eqs. (20). In this way, the residuals turn out to be the first-order-filtered estimation of $f_{ext,t}$, $m_{ext,c}$, τ^*_{ext} only due to the unexpected collision, and they can be used for detection and isolation. As regards the reaction, if the task allows a safe release of the target, the end-effector could perform it and the system can follow the proposed reaction strategy. On the other hand, in case the task is critical and it is not safe to release immediately the target, the redundancy of the system could be exploited to

change the configuration of the arm and move the base to escape from the contact, while keeping the same pose of the end-effector. This scenario is worth a deeper analysis, which is left for future work.

Another open issue is the case with multiple unexpected contacts at the same time. Indeed, the observer would estimate and locate only the force resultant, which can not be used for a safe reaction in every circumstance. Additional information would be required to identify each force acting on the system, and consequently an effective escape direction to move.

The other main assumption in this work is the rigidity of the system. Actually, space robots have flexible components, such as the joint transmission and the links. The proposed strategy can be easily extended to robots with flexible joints equipped with torque sensors. Indeed, in the observer, the measured joint torques can be used in place of the commanded torques for the rigid model, as shown in [26] for fixed-base robots. For the control, the availability of torque sensors enables to implement torque control loop, and thus to use the proposed reaction strategy. Note that torque sensors are suggested in scenarios involving contact situations since they can be effectively used to implement compliant controllers [46]. Regarding the flexibility at link level, further analyses are necessary and they will be addressed in future work. It is expected that the reaction control can be integrated with techniques dedicated to suppress vibrations, e.g., acting at setpoint level as [47]. Considering the rigid-model-based observer, the effects of vibration on the estimation of the force will be assessed. Proper tuning of the gains may mitigate them to some extent. Alternatively, the links deflection could be approximated introducing new coordinates and its contribution added to the generalized momenta, which are used for the computation of the residuals. The feasibility of this possible solution will be assessed in future research.

VIII. Conclusions

In this paper, the unexpected collision handling problem for free-flying orbital robots has been addressed. In particular, a nonlinear observer to detect, isolate and estimate the contact has been proposed. It is based on a formulation of the dynamics, in which the velocity of the center of mass (CoM) of the whole system, the angular velocity of the spacecraft and the joint velocities are used as generalized velocities. Then, a compliant controller has been developed to react to the collision. Thanks to the proposed control strategy the build-up of the contact force and instability in the post-impact phase are avoided. It has been proved that the controlled system is input-to-state stable. Finally, the performance of the observer and controller has been assessed through a numerical example, considering a 7 degrees of freedom (DoF) arm on a spacecraft equipped with thrusters and variable speed control moment gyros (VSCMG). In the simulation, the reaction controller has been integrated with the control proposed in [29], leading to a control system capable of operating in both nominal and emergency conditions, and saving fuel in contact-free end-effector maneuvering. Future work will address the open issues described in Sect. VII and the proposed strategy will be validated on real hardware, e.g., on the On-Orbit Servicing (OOS) simulator facility of the DLR.

Appendix

A. Derivation of the relations (16)

In order to derive the relation $\tilde{C}_{cr}\omega_b + \tilde{C}_{cm}\dot{q} = 0$, it is sufficient to write the time derivative of the translational momentum in the inertial frame and compare it to the first row of Eq. (13). Indeed,

$$\dot{h}_t^t = m\dot{v}_c = f_{t,tot}, \tag{A.1}$$

where $f_{t,tot} \in \mathbb{R}^3$ is the total force in the inertial frame, thus including f_t and $f_{ext,t}$. Therefore, comparing Eq. (A.1) and the first row of Eq. (13), the relation $\tilde{C}_{cr}\omega_b + \tilde{C}_{cm}\dot{q} = 0$ can be obtained. A similar result is obtained also in [48].

The relation (16a) can be derived computing the time derivative of the rotational momentum around C and expressed in C

$$\dot{h}_c^r + [\omega_b]^\wedge h_c^r = m_{c,tot}, \tag{A.2}$$

where $m_{c,tot} \in \mathbb{R}^3$ is the total centroidal torque acting on the system, and thus including m_c and $m_{ext,c}$. Then, considering that $h_c^r = I_c\omega_b + I_c\bar{J}_\omega\dot{q}$, it is possible to write

$$I_c\dot{\omega}_b + I_c\bar{J}_\omega\ddot{q} + \dot{I}_c\omega_b + \dot{I}_c\bar{J}_\omega\dot{q} + I_c\dot{\bar{J}}_\omega\dot{q} + [\omega_b]^\wedge(I_c\omega_b + I_c\bar{J}_\omega\dot{q}) = m_{c,tot}. \tag{A.3}$$

Again, comparing Eq. (A.3) with the second row of Eq. (13), the relation (16a) is derived.

Finally, regarding the relation (16b), a quasi-Lagrangian approach [49] is used to rederive the joints equation in Eq. (13). Then, the relation (16b) is obtained by comparison of the quasi-Lagrangian joints formulation with the third row of Eq. (13). This approach is necessary because not all the variables used to express the dynamics are integrable. In particular, this is the case of the velocity ω_b, which is called quasi-velocity. In order to derive the dynamic equations, integrable coordinates are required, and thus the generalized coordinates $y \in \mathbb{R}^{6+n}$ are defined, whose derivatives are:

$$\begin{bmatrix} v_c \\ \omega_b \\ \dot{q} \end{bmatrix} = \begin{bmatrix} E & 0 & 0 \\ 0 & J_\Phi^{-1} & 0 \\ 0 & 0 & E \end{bmatrix} \begin{bmatrix} \dot{p}_{tc} \\ \dot{\Phi} \\ \dot{q} \end{bmatrix} = \Xi^T \dot{y}. \tag{A.4}$$

where $\Phi \in \mathbb{R}^3$, $\dot{\Phi} \in \mathbb{R}^3$ are the Euler angle vector and its time derivative, respectively; $J_\Phi \in \mathbb{R}^{3\times3}$ is the Jacobian mapping ω_b in $\dot{\Phi}$. The matrix Ξ is function of the generalized coordinates y. Note that any rotation parameterization different from the Euler angles can be used without affecting the following joints dynamics derivation.

Introducing $x = [v_c^T \ \omega_b^T \ \dot{q}^T]^T \in \mathbb{R}^{6+n}$, the following relation can be written:

$$\dot{y} = \Omega x \tag{A.5}$$

where $\Omega = \Xi^{-T} \in \mathbb{R}^{(6+n)\times(6+n)}$.

Exploiting Eqs. (A.4)-(A.5), the quasi-Lagrangian formulation can be derived from the standard one [49], resulting in

$$\delta y^T \left(\Xi \frac{d}{dt} \left[\frac{\partial T}{\partial x} \right] + \dot{\Xi} \frac{\partial T}{\partial x} - \frac{\partial T}{\partial y} - H \frac{\partial T}{\partial x} - Q \right) = 0, \tag{A.6}$$

where

$$H = \begin{bmatrix} x^T \Omega^T \frac{\partial \Xi}{\partial y_1} \\ \vdots \\ x^T \Omega^T \frac{\partial \Xi}{\partial y_{6+n}} \end{bmatrix} \in \mathbb{R}^{(6+n)\times(6+n)}, \tag{A.7}$$

and where $Q \in \mathbb{R}^{6+n}$ is the vector of the generalized forces, $T \in \mathbb{R}$ is the kinetic energy of the system expressed in terms of x. The potential energy is assumed to be zero.

Theoretically, Eq. (A.6) should be used to derive the dynamics equations of the system. However, it can be noticed that the relations in Eq. (A.4) are completely decoupled, which, in particular, means that the joints coordinates are not associated with nonholonomic relations. Consequently, for these degrees of freedom, the general equation (A.6) is simply the standard Lagrange equation [49]. Hence, it is possible to proceed in the following way.

First, the kinetic energy is computed as follows

$$T = \frac{1}{2}(m v_c^T v_c + \breve{\omega}^T M^* \breve{\omega}). \tag{A.8}$$

Then, the Lagrange formalism is applied to derive the joints dynamics, and the following equation is obtained:

$$\tilde{M}_m \ddot{q} + \bar{J}_\omega^T I_c^T \dot{\omega}_b + (\dot{\tilde{M}}_m - \frac{1}{2}\tilde{M}_{rm/q} - \frac{1}{2}\tilde{M}_{m/q})\dot{q} + (\dot{\bar{J}}_\omega^T I_c^T + \bar{J}_\omega^T \dot{I}_c^T + \frac{1}{2}I_{c/q}^{-T} I_c^T - \frac{1}{2}\bar{J}_{\omega/q}^T I_c^T)\omega_b = \bar{\tau}_{tot}^*, \tag{A.9}$$

where $\tilde{M}_{m/q}$ and $\tilde{M}_{rm/q}$ are defined in Eq. (17). In (A.9), the following relations have been used

$$\begin{bmatrix} \omega_b^T \frac{\partial I_c^T}{\partial q_1} \\ \vdots \\ \omega_b^T \frac{\partial I_c^T}{\partial q_n} \end{bmatrix} + \begin{bmatrix} \dot{q}^T \bar{J}_\omega^T \frac{\partial I_c^T}{\partial q_1} \\ \vdots \\ \dot{q}^T \bar{J}_\omega^T \frac{\partial I_c^T}{\partial q_n} \end{bmatrix} + \begin{bmatrix} \dot{q}^T \frac{\partial \bar{J}_\omega^T}{\partial q_1} I_c^T \\ \vdots \\ \dot{q}^T \frac{\partial \bar{J}_\omega^T}{\partial q_n} I_c^T \end{bmatrix} = \bar{J}_{\omega/q}^T I_c^T - I_{c/q}^{-T} I_c^T, \tag{A.10}$$

where $I_{c/q}^{-T}$ and $\bar{J}_{\omega/q}^{T}$ are defined in Eq. (18).

From the comparison between Eq. (A.9) and the third row of Eq. (13), the relation (16b) can be derived.

B. Proof of the property $\breve{\omega}^T (\dot{M}^* - 2C^*)\breve{\omega} = 0$

It is well known that for the dynamics (2) the property $v^T (\dot{M} - 2C)v = 0$ is valid, with $v = [v_b^T \ \omega_b^T \ \dot{q}^T]^T$, and it is transferred to the dynamics (13) thanks to the chosen transformation (9) [39], and thus

$$
\begin{bmatrix} v_c^T & \omega_b^T & \dot{q}^T \end{bmatrix} \left(\begin{bmatrix} \mathbf{0} & \mathbf{0} & \mathbf{0} \\ \mathbf{0} & \dot{I}_c & \dot{I}_c \bar{J}_\omega + I_c \dot{\bar{J}}_\omega \\ \mathbf{0} & \dot{\bar{J}}_\omega^T I_c^T + \bar{J}_\omega^T \dot{I}_c^T & \dot{M}_m \end{bmatrix} - 2 \begin{bmatrix} \mathbf{0} & \tilde{C}_{cr} & \tilde{C}_{cm} \\ -\tilde{C}_{cr}^T & \tilde{C}_r & \tilde{C}_{rm} \\ -\tilde{C}_{cm}^T & \tilde{C}_{mr}^T & \tilde{C}_m \end{bmatrix} \right) \begin{bmatrix} v_c \\ \omega_b \\ \dot{q} \end{bmatrix} = 0.
$$

(B.11)

Considering the relations (16) proven in Sect. A of the Appendix, it is possible to write

$$
\begin{bmatrix} v_c^T & \omega_b^T & \dot{q}^T \end{bmatrix} \begin{bmatrix} \mathbf{0} & \tilde{C}_{cr} & \tilde{C}_{cm} \\ -\tilde{C}_{cr}^T & \tilde{C}_r & \tilde{C}_{rm} \\ -\tilde{C}_{cm}^T & \tilde{C}_{mr} & \tilde{C}_m \end{bmatrix} \begin{bmatrix} v_c \\ \omega_b \\ \dot{q} \end{bmatrix} = \begin{bmatrix} v_c^T & \breve{\omega}^T \end{bmatrix} \begin{bmatrix} \mathbf{0} & \mathbf{0} \\ \mathbf{0} & C^* \end{bmatrix} \begin{bmatrix} v_c \\ \breve{\omega} \end{bmatrix}.
$$

(B.12)

Since the inertia matrix is the same for the dynamics (13) and (32), exploiting the relations (B.11) in (B.12), it is possible to conclude that the property $\breve{\omega}^T (\dot{M}^* - 2C^*)\breve{\omega} = 0$ is valid for the dynamics (32b).

References

[1] Miller, R., Minsky, M. L., and Smith, D. B., "Space Applications of Automation, Robotics and Machine Intelligence Systems (ARAMIS). Volume 1: Executive Summary," 1982.

[2] Rembala, R., and Ower, C., "Robotic assembly and maintenance of future space stations based on the ISS mission operations experience," *Acta Astronautica*, Vol. 65, No. 7-8, 2009, pp. 912–920. https://doi.org/10.1016/j.actaastro.2009.03.064.

[3] Sallaberger, C., "Canadian space robotic activities," *Acta astronautica*, Vol. 41, No. 4-10, 1997, pp. 239–246. https://doi.org/10.1016/S0094-5765(98)00082-4.

[4] Sato, N., and Doi, S., "JEM Remote Manipulator System (JEMRMS) Human-In-the-Loop Test," *International Symposium on Space Technology and Science, 22 nd, Morioka, Japan*, 2000, pp. 1195–1199.

[5] Didot, F., Oort, M., Kouwen, J., and Verzijden, P., "The ERA system: Control architecture and performance results," *Proc. 6th International Symposium on Artificial Intelligence, Robotics and Automation in Space (i-SAIRAS), Montral, Canada*, Citeseer, 2001.

[6] Oda, M., Kibe, K., and Yamagata, F., "ETS-VII, space robot in-orbit experiment satellite," *Proceedings of IEEE international conference on robotics and automation*, Vol. 1, IEEE, 1996, pp. 739–744. https://doi.org/10.1109/ROBOT.1996.503862.

[7] Friend, R. B., "Orbital express program summary and mission overview," *Sensors and systems for space applications II*, Vol. 6958, International Society for Optics and Photonics, 2008, p. 695803. https://doi.org/10.1117/12.783792.

[8] Yoshida, K., Sashida, N., Kurazume, R., and Umetani, Y., "Modeling of collision dynamics for space free-floating links with extended generalized inertia tensor," *Robotics and Automation, 1992. Proceedings., 1992 IEEE International Conference on*, IEEE, 1992, pp. 899–904. https://doi.org/10.1109/ROBOT.1992.220182.

[9] Cyril, X., Jaar, G. J., and Misra, A. K., "The effect of payload impact on the dynamics of a space robot," *Intelligent Robots and Systems' 93, IROS'93. Proceedings of the 1993 IEEE/RSJ International Conference on*, Vol. 3, IEEE, 1993, pp. 2070–2075. https://doi.org/10.1109/IROS.1993.583916.

[10] Wee, L.-B., and Walker, M. W., "On the dynamics of contact between space robots and configuration control for impact minimization," *IEEE Transactions on Robotics and Automation*, Vol. 9, No. 5, 1993, pp. 581–591. https://doi.org/10.1109/70.258051.

[11] Nenchev, D. N., and Yoshida, K., "Impact analysis and post-impact motion control issues of a free-floating space robot subject to a force impulse," *IEEE Transactions on Robotics and Automation*, Vol. 15, No. 3, 1999, pp. 548–557. https://doi.org/10.1109/70.768186.

[12] Yoshida, K., Dimitrov, D., and Nakanishi, H., "On the capture of tumbling satellite by a space robot," *Intelligent robots and systems, 2006 IEEE/RSJ international conference on*, IEEE, 2006, pp. 4127–4132. https://doi.org/10.1109/IROS.2006.281900.

[13] Yoshida, K., Nakanishi, H., Ueno, H., Inaba, N., Nishimaki, T., and Oda, M., "Dynamics, control and impedance matching for robotic capture of a non-cooperative satellite," *Advanced Robotics*, Vol. 18, No. 2, 2004, pp. 175–198. https://doi.org/10.1163/156855304322758015.

[14] Abiko, S., Lampariello, R., and Hirzinger, G., "Impedance control for a free-floating robot in the grasping of a tumbling target with parameter uncertainty," *Intelligent Robots and Systems, 2006 IEEE/RSJ International Conference on*, IEEE, 2006, pp. 1020–1025. https://doi.org/10.1109/IROS.2006.281785.

[15] Giordano, A. M., Garofalo, G., and Albu-Schaffer, A., "Momentum dumping for space robots," *Decision and Control (CDC), 2017 IEEE 56th Annual Conference on*, IEEE, 2017, pp. 5243–5248. https://doi.org/10.1109/CDC.2017.8264434.

[16] Haddadin, S., De Luca, A., and Albu-Schäffer, A., "Robot collisions: A survey on detection, isolation, and identification," *IEEE Transactions on Robotics*, Vol. 33, No. 6, 2017, pp. 1292–1312. https://doi.org/10.1109/TRO.2017.2723903.

[17] Ren, T., Dong, Y., Wu, D., and Chen, K., "Collision detection and identification for robot manipulators based on extended state observer," *Control Engineering Practice*, Vol. 79, 2018, pp. 144–153. https://doi.org/j.conengprac.2018.07.004.

[18] Flacco, F., Paolillo, A., and Kheddar, A., "Residual-based contacts estimation for humanoid robots," *Humanoid Robots (Humanoids), 2016 IEEE-RAS 16th International Conference on*, IEEE, 2016, pp. 409–415. https://doi.org/10.1109/HUMANOIDS.2016.7803308.

[19] Vorndamme, J., Schappler, M., and Haddadin, S., "Collision detection, isolation and identification for humanoids," *2017 IEEE International Conference on Robotics and Automation (ICRA)*, IEEE, 2017, pp. 4754–4761. https://doi.org/10.1109/ICRA.2017.7989552.

[20] Tomić, T., and Haddadin, S., "Simultaneous estimation of aerodynamic and contact forces in flying robots: Applications to metric wind estimation and collision detection," *Robotics and Automation (ICRA), 2015 IEEE International Conference on*, IEEE, 2015, pp. 5290–5296. https://doi.org/10.1109/ICRA.2015.7139937.

[21] Tomić, T., Ott, C., and Haddadin, S., "External wrench estimation, collision detection, and reflex reaction for flying robots," *IEEE Transactions on Robotics*, Vol. 33, No. 6, 2017, pp. 1467–1482. https://doi.org/10.1109/TRO.2017.2750703.

[22] Dahiya, R. S., Mittendorfer, P., Valle, M., Cheng, G., and Lumelsky, V. J., "Directions toward effective utilization of tactile skin: A review," *IEEE Sensors Journal*, Vol. 13, No. 11, 2013, pp. 4121–4138. https://doi.org/10.1109/JSEN.2013.2279056.

[23] De Maria, G., Natale, C., and Pirozzi, S., "Force/tactile sensor for robotic applications," *Sensors and Actuators A: Physical*, Vol. 175, 2012, pp. 60–72. https://doi.org/j.sna.2011.12.042.

[24] Lumelsky, V. J., and Cheung, E., "Real-time collision avoidance in teleoperated whole-sensitive robot arm manipulators," *IEEE Transactions on Systems, Man, and Cybernetics*, Vol. 23, No. 1, 1993, pp. 194–203. https://doi.org/10.1109/21.214777.

[25] Cavenago, F., Giordano, A. M., and Massari, M., "Contact force observer for space robots," *2019 IEEE 58th Conference on Decision and Control (CDC)*, IEEE, 2019, pp. 2528–2535. https://doi.org/10.1109/CDC40024.2019.9029285.

[26] De Luca, A., Albu-Schaffer, A., Haddadin, S., and Hirzinger, G., "Collision detection and safe reaction with the DLR-III lightweight manipulator arm," *2006 IEEE/RSJ International Conference on Intelligent Robots and Systems*, IEEE, 2006, pp. 1623–1630. https://doi.org/10.1109/IROS.2006.282053.

[27] Flores-Abad, A., Nandayapa, M., and Garcia-Teran, M. A., "Force sensorless impedance control for a space robot to capture a satellite for on-orbit servicing," *2018 IEEE Aerospace Conference*, IEEE, 2018. https://doi.org/10.1109/AERO.2018.8396710.

[28] Moosavian, S. A. A., and Papadopoulos, E., "On the control of space free-flyers using multiple impedance control," *Robotics and Automation, 1997. Proceedings., 1997 IEEE International Conference on*, Vol. 1, IEEE, 1997, pp. 853–858. https://doi.org/10.1109/ROBOT.1997.620141.

[29] Giordano, A. M., Ott, C., and Albu-Schäffer, A., "Coordinated Control of Spacecraft's Attitude and End-Effector for Space Robots," *IEEE Robotics and Automation Letters*, Vol. 4, No. 2, 2019, pp. 2108–2115. https://doi.org/10.1109/LRA.2019.2899433.

[30] Giordano, A. M., Dietrich, A., Ott, C., and Albu-Schäffer, A., "Coordination of thrusters, reaction wheels, and arm in orbital robots," *Robotics and Autonomous Systems*, 2020, p. 103564. https://doi.org/j.robot.2020.103564.

[31] Murray, R. M., *A mathematical introduction to robotic manipulation*, CRC press, 2017, pp. 53–57.

[32] Giordano, A. M., Calzolari, D., and Albu-Schäffer, A., "Workspace fixation for free-floating space robot operations," *Robotics and Automation (ICRA), 2018 IEEE International Conference on*, IEEE, 2018. https://doi.org/10.1109/ICRA.2018.8460478.

[33] Khalil, H. K., *Nonlinear systems, 3rd ed.*, Prentice-Hall, 2002, pp. 174–180.

[34] Angeli, D., "Input-to-state stability of PD-controlled robotic systems," *Automatica*, Vol. 35, No. 7, 1999, pp. 1285–1290. https://doi.org/10.1016/S0005-1098(99)00037-0.

[35] From, P. J., Gravdahl, J. T., Pettersen, K. Y., et al., *Vehicle-manipulator systems*, Springer, 2016, pp. 285–304.

[36] Yoon, H., and Tsiotras, P., "Spacecraft adaptive attitude and power tracking with variable speed control moment gyroscopes," *Journal of Guidance, Control, and Dynamics*, Vol. 25, No. 6, 2002, pp. 1081–1090. https://doi.org/10.2514/2.4987.

[37] Antonello, A., Valverde, A., and Tsiotras, P., "Dynamics, Control, and Trajectory Tracking of Spacecraft Manipulators with Thrusters and Momentum Exchange Devices," *AIAA Journal of Guidance, Control, and Dynamics*, Vol. 42, No. 1, 2019, pp. 15–29. https://doi.org/10.2514/1.G003601.

[38] Oestersötebier, F., Wang, P., and Trächtler, A., "A Modelica Contact Library for Idealized Simulation of Independently Defined Contact Surfaces," *Proceedings of the 10 th International Modelica Conference; March 10-12; 2014; Lund; Sweden*, Linköping University Electronic Press, 2014, pp. 929–937. https://doi.org/10.3384/ecp14096929.

[39] Garofalo, G., Ott, C., and Albu-Schäffer, A., "On the closed form computation of the dynamic matrices and their differentiations," *2013 IEEE/RSJ International Conference on Intelligent Robots and Systems*, IEEE, 2013, pp. 2364–2359. https://doi.org/10.1109/IROS.2013.6696688.

[40] Crassidis, J. L., and Markley, F. L., "Unscented filtering for spacecraft attitude estimation," *Journal of guidance, control, and dynamics*, Vol. 26, No. 4, 2003, pp. 536–542. https://doi.org/10.2514/2.5102.

[41] Gallardo, A. P., Mishra, H., Giordano, A. M., and Lampariello, R., "Robust Estimation of Motion States for Free-Floating Tumbling Target Capture," *2019 IEEE Aerospace Conference*, IEEE, 2019, pp. 1–11. https://doi.org/10.1109/AERO.2019.8741802.

[42] Crassidis, J. L., "Sigma-point Kalman filtering for integrated GPS and inertial navigation," *IEEE Transactions on Aerospace and Electronic Systems*, Vol. 42, No. 2, 2006, pp. 750–756. https://doi.org/10.1109/TAES.2006.1642588.

[43] Gil-Fernández, J., Prieto-Llanos, T., Panzeca, R., and Drai, R., "Autonomous gnc algorithms for neo impactor missions," *Proceedings of the 20th International Symposium on Space Flight Dynamics*, 2007, pp. 1–14.

[44] Cavenago, F., Di Lizia, P., Massari, M., and Wittig, A., "On-board spacecraft relative pose estimation with high-order extended Kalman filter," *Acta Astronautica*, Vol. 158, 2019, pp. 55–67. https://doi.org/j.actaastro.2018.11.020.

[45] Aghili, F., and Parsa, K., "Adaptive motion estimation of a tumbling satellite using laser-vision data with unknown noise characteristics," *2007 IEEE/RSJ International Conference on Intelligent Robots and Systems*, IEEE, 2007, pp. 839–846. https://doi.org/10.1109/IROS.2007.4399143.

[46] Albu-Schäffer, A., Ott, C., and Hirzinger, G., "A unified passivity-based control framework for position, torque and impedance control of flexible joint robots," *The international journal of robotics research*, Vol. 26, No. 1, 2007, pp. 23–39. https://doi.org/10.1177/0278364907073776.

[47] O'Connor, W. J., de la Flor, F. R., McKeown, D. J., and Feliu, V., "Wave-based control of non-linear flexible mechanical systems," *Nonlinear Dynamics*, Vol. 57, No. 1-2, 2009, p. 113. https://doi.org/10.1007/s11071-008-9425-4.

[48] Garofalo, G., Henze, B., Englsberger, J., and Ott, C., "On the inertially decoupled structure of the floating base robot dynamics," *IFAC-PapersOnLine*, Vol. 48, Elsevier, 2015, pp. 322–327. https://doi.org/j.ifacol.2015.05.189.

[49] Cameron, J. M., and Book, W. J., "Modeling mechanisms with nonholonomic joints using the Boltzmann-Hamel equations," *The International Journal of Robotics Research*, Vol. 16, No. 1, 1997, pp. 47–59. https://doi.org/10.1177/027836499701600104.